Flagellar Motility in Bacteria: Structure and Function of Flagellar Motor

Hiroyuki Terashima,* Seiji Kojima,* *and* Michio Homma*

Contents

Abstract

Bacterial flagella are filamentous organelles that drive cell locomotion. They thrust cells in liquids (swimming) or on surfaces (swarming) so that cells can move toward favorable environments. At the base of each flagellum, a reversible rotary motor, which is powered by the proton- or the sodium-motive force,

* Division of Biological Science, Graduate School of Science, Nagoya University, Nagoya, Japan

is embedded in the cell envelope. The motor consists of two parts: the rotating part, or rotor, that is connected to the hook and the filament, and the nonrotating part, or stator, that conducts coupling ion and is responsible for energy conversion. Intensive genetic and biochemical studies of the flagellum have been conducted in *Salmonella typhimurium* and *Escherichia coli*, and more than 50 gene products are known to be involved in flagellar assembly and function. The energy-coupling mechanism, however, is still not known. In this chapter, we survey our current knowledge of the flagellar system, based mostly on studies from *Salmonella*, *E. coli*, and marine species *Vibrio alginolyticus*, supplemented with distinct aspects of other bacterial species revealed by recent studies.

Key Words: Proton motive force, Sodium motive force, Energy transduction, *Vibrio alginolyticus*, *Salmonella typhimurium*, *Escherichia coli*.   © 2008 Elsevier Inc.

1. Introduction

1.1. Molecular architecture of flagella

The flagellum consists of three parts: the filament (helical propeller), the hook (universal joint), and the basal structure (rotary motor) (Fig. 2.1). The largest part of the flagellum is the filament, a helical structure whose shape can vary among different helical forms, a phenomenon termed polymorphism (Asakura, 1970). This polymorphic alteration of flagellar shape is associated with phase variation (Iino, 1969). When the cell swims, the flagellar filament serves as a screw propeller to convert rotary motion of the motor into thrust (Berg and Anderson, 1973). In *Salmonella*, it grows to a length of around 15 μm and is composed of as many as 30,000 copies of a single protein named flagellin (Minamino and Namba, 2004). Some bacteria, for example *Vibrio*, have several closely related flagellins that form the filament (McCarter, 2001). The flagellin subunits (FliC in *Escherichia coli* and *Salmonella*) are self-assembled to form a hollow concentric double-tubular structure (inner and outer tubes) consisting of 11 protofilaments, which are arranged approximately parallel to the filament axis (Mimori *et al.*, 1995; Morgan *et al.*, 1995). Formation of a helical structure is achieved by a mixture of the protofilaments of two distinct conformations, the R- and L-type, distinguished by their helical handedness right or left (Asakura, 1970; Calladine, 1978). Each protofilament switches between these two conformations by responding to a variety of factors including pH, ionic strength, mechanical stress, and mutations (Kamiya and Asakura, 1976; Macnab and Ornston, 1977). Later, X-ray fiber diffraction studies revealed slightly different subunit packing between the R- and L-type, whose repeat distances are 51.9 and 52.7 Å, respectively (Yamashita *et al.*, 1998). To
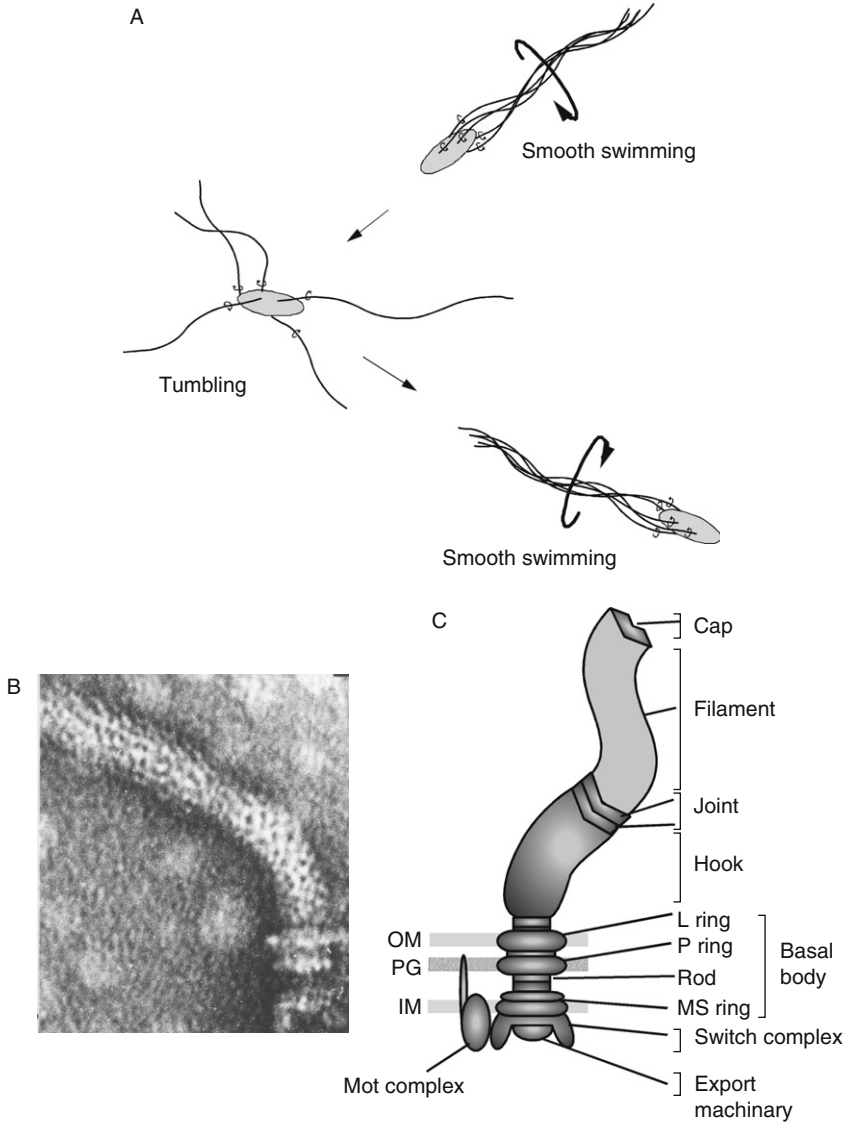
Figure 2.1 **(A) Behavior of bacterial cells. (B) Electron micrograph of flagella isolated from *Salmonella typhimurium*. (C) Schematic diagram of flagellar structure of Gram-negative bacteria.**

understand the polymorphic switching mechanism, the crystal structure of fragment containing most of the flagellin protein (F41 fragment of FliC) was solved at 2 Å (Samatey *et al.*, 2001). In the crystal, F41 fragments of the R-type conformation form protofilaments arranged in an antiparallel

manner, and simulation using atomic model revealed that a small, distinct conformational changes in the β–hairpin in D1, the domain that contributes to outer tube structure, is responsible for the conformational switching between L– and R–type protofilament. The crystal structure of F41 fragment lacks the D0 domain that forms inner tube structure. Later, electron cryomicroscopy and helical image analysis made it possible to build complete atomic model of the R–type filament structure including D0 domain of flagellin, revealing that intersubunit hydrophobic interactions in the inner tube (domain D0) make the filament structure mechanically stable, and the diameter of central channel is only 2 nm (Yonekura *et al.*, 2003). This central channel serves as a transport pathway of flagellins that will polymerize at the tip of the growing filament (Fig. 2.2).

The base of the filament is connected to the short tubular structure called the hook, which is thought to function as a universal joint to smoothly transmit the torque produced by the motor to the filament. The hook structure of *Salmonella* is composed of about 120 copies of a single protein FlgE and its length is controlled at 55 ($\pm$6) nm (Hirano *et al.*, 1994). The core structure of the hook protein was solved by X–ray crystallography, and its atomic model was docked onto the density map of the hook obtained by electron cryomicroscopy (Samatey *et al.*, 2004).

The junction between hook and filament consists of the two proteins, FlgK (HAP1) and FlgL (HAP3) (Homma and Iino, 1985; Ikeda *et al.*, 1985). About 13 molecules of each protein are present in each flagellum (Ikeda *et al.*, 1987). Mutational studies suggested that the junction acts as a buffering structure connecting two filamentous structures (hook and filament) with distinct mechanical properties (Fahrner *et al.*, 1994).

The proximal end of the hook is connected to the basal body structure, consisting of the rod and three coaxially mounted rings, termed as MS, P, and L ring. The MS ring is embedded in the cytoplasmic membrane and made of a single protein FliF (Ueno *et al.*, 1992), the P and L rings are associated with the peptidoglycan layer and the outer membrane, respectively, and are composed of FlgI and FlgH (Homma *et al.*, 1987; Schoenhals and Macnab, 1996). The rod structure is composed of three proximal rod proteins FlgB, FlgC, FlgF, and a distal rod protein FlgG, and fully traverses the periplasmic space. The L and P rings together form a quite rigid assembly resistant to stringent chemical treatments, and the LP–ring complex is believed to act as a molecular bushing for the flagellar axial structure (Akiba *et al.*, 1991). The basal body of Gram–positive bacteria is composed of only the MS ring and rod, and the LP ring is not present (Kobayashi *et al.*, 2003), probably because Gram–positive bacteria do not have the outer membrane but have a thick peptidoglycan layer. When the basal body is isolated with more gentle treatment, a drum–shaped structure, called C ring, was found on the MS ring facing the cytoplasm (Francis *et al.*, 1994). It is composed mostly of FliM and FliN proteins (Thomas *et al.*, 2006; Zhao
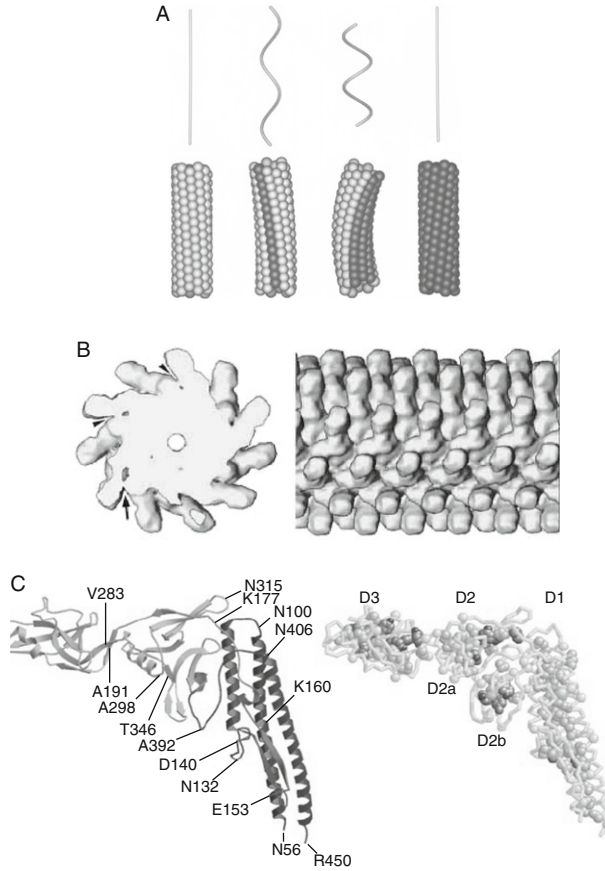
Figure 2.2 (A) Polymorphic structure of the flagellar filament. The filaments of L-type straight, normal, curly, and R-type straight are shown by the left to right in this order. (B) The flagellar filament structure revealed by electron cryomicroscopy. The end-on view of the cross section (left) and the side view of long segment (right). (C) The backbone trace of the flagellin (FliC) molecule of *Salmonella typhimurium*. The figures were kindly supplied by K. Namba.

et al., 1996a,b). These proteins, together with FliG which is located beneath the MS ring, have been known to form a complex, referred to as the switch complex. Mutations in each of these three proteins cause defects in switching the rotational direction of the motor (Yamaguchi *et al.*, 1986a). They are also important for rotation, and mutational studies revealed that FliG most closely participates in torque generation (Lloyd *et al.*, 1996). Careful preparation of the basal structure further revealed a central protrusion within the C ring, that is probably the export apparatus essential for assembly of flagellum (Katayama *et al.*, 1996).

1.2. Gene regulation

More than 50 genes are required for flagellar formation and function (Macnab, 2003). Because the flagellum is such a big organelle, a large amount of energy is consumed during the assembly process. Bacteria deal with this problem by developing highly organized and regulated systems for flagellar assembly. Its characteristic feature is that the flagellar gene regulation temporally and tightly couples to the assembly process. Here we survey this regulatory mechanism in *Salmonella*, which has been most extensively studied. For further details of flagellar gene regulations in *Salmonella enterica* serovar *typhimurium* and *E. coli* as well as the other bacteria, such as *Caulobacter cresentus* and *Vibrio* spp., see the reviews cited in Chilcott and Hughes (2000), McCarter (2004), Wolfe and Visick (2008), and Wu and Newton (1997).

In *Salmonella*, the flagellar/motility/chemotaxis genes constitute a regulon, and they are arranged in hierarchical order into three classes, early, middle, and late (Fig. 2.3) (Kutsukake *et al.*, 1990). At the top of the hierarchy is a single operon (class 1 master operon) containing the *flhDC* genes (Liu and Matsumura, 1994). The FlhC and FlhD proteins form a heterotetrametic complex $FlhC_2FlhD_2$ that direct σ^{70}-RNA polymerase complex to activate transcription from class 2 promoters upstream of the
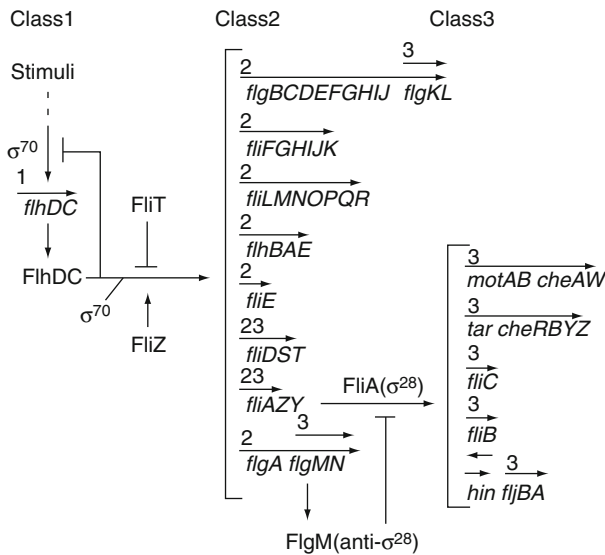

Figure 2.3   Regulation of transcription of the flagellar regulon. The flagellar operons are indicated by arrows. The numbers on the arrows show the class of transcriptional hierarchy in the flagellar regulon. Descriptions of the transcriptional regulation and the function of the gene products are described in text.

middle gene operons. The *flhDC* operon is tightly regulated under the control of a number of global regulatory signals such as cAMP-CRP, heat shock, DNA supercoiling, growth phase, surface–liquid transition, ClpXP protease, and c-di–GMP (reviewed in Chilcott and Hughes, 2000; Wolfe and Visick, 2008). Expression of *flhDC* is also linked to the cell cycle, showing that flagellation and cell cycle are interdependent processes (Pruss and Matsumura, 1996, 1997).

More than 30 middle gene products from class 2 operons are primarily required for the structure and assembly of the hook and basal body, and include regulatory proteins that control transcription of the genes from class 3 operons. Class 3 operons encode for proteins required late in the assembly process, including flagellin, hook-associated proteins (HAPs), stator components, and chemosensory systems. Expression of class 3 operons is positively controlled by FliA and negatively by FlgM (Gillen and Hughes, 1991; Kutsukake and Iino, 1994). FliA is the flagellum-specific transcription factor σ^{28} (Ohnishi *et al.*, 1990), and it leads σ^{28}-RNA polymerase complex to transcribe class 3 late gene operons, whereas FlgM is an anti-σ^{28} factor specific for FliA (Ohnishi *et al.*, 1992). Since filament formation requires large resources of the cells, the stage to initiate expression of class 3 operons is a critical checkpoint for flagellar gene regulation. Actually, what happens *in vivo* is that the late genes are not transcribed until the assembly of hook-basal body structures has been completed. Mutations in any one of the hook-basal body genes prevent the transcription of class 3 operons to avoid unnecessary late gene expression that would cause an energy drain in the cell. This remarkable coupling between structure and gene expression is achieved by the balance of FliA and FlgM. FlgM inhibits FliA for the expression of class 3 operons until hook-basal body completion, at which time FlgM is secreted out from the cells through hook-basal body structure and released FliA turns on transcription of class 3 operons to achieve filament formation and motor assembly (Hughes *et al.*, 1993; Kutsukake, 1994). Such a controlled expression is coupled to the ordered secretion of each gene products by the flagellum-specific export apparatus, putatively located inside of the MS ring, to complete the self-assembly of flagella.

As described above, sensing hook-basal body completion followed by FlgM secretion is such a critical checkpoint; *Salmonella* utilizes another factor involved in negative regulation in FlgM secretion. This gene, *flk* (Karlinsey *et al.*, 1997), also called as *rflH* (Kutsukake, 1997), was identified as the factor that allows expression of class 3 operons only when mutated in strains defective in LP ring assembly. Flk is a cytoplasmic-facing protein anchored to the inner membrane by a single, C-terminal transmembrane domain, and it was revealed that turnover of FlgM was increased in *flk* background due to FlgM secretion into periplasm where it is degraded, suggesting that Flk prevents premature secretion of the FlgM into periplasm, thus acting as a braking systems for the flagellar export system

(Aldridge *et al.*, 2006). Loss of only Flk does not show any phenotype related to motility, and *flk* gene is not located in the flagellar regulon, so the role of Flk in the wild-type cell is still unclear (Karlinsey *et al.*, 1997; Kutsukake, 1997).

1.3. Flagellar assembly

As described in Section 1.2, flagellar assembly is tightly coupled to the gene expression, and the monitoring system at the stage of hook completion allows cells to achieve efficient and economical filament formation. The sequence of events in flagellar assembly has been extensively studied in *Salmonella* and *E. coli* by studying partial structures of flagella from mutants defective in a certain flagellar gene (Kubori *et al.*, 1992; Suzuki and Komeda, 1981; Suzuki *et al.*, 1978). In general, assembly starts at the inner structure of the basal body then proceeds to the outer ones (Fig. 2.4). The first built structure is the MS ring and proximal rod, which is formed by a single protein FliF (Ueno *et al.*, 1992). The MS ring is the core structure of the rotor and is embedded in the cytoplasmic membrane. The C ring attaches on

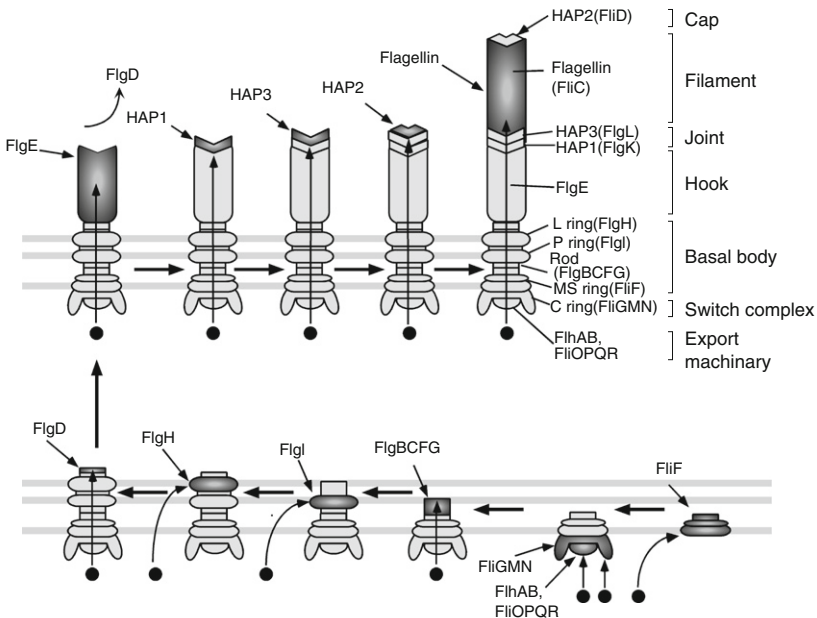**Figure 2.4** Morphological assembly of bacterial flagellum. The model of pathway is created based on the assumption that the structure is built from a simple to complicated form. The flagellar morphogenesis is thought to begin with the formation of MS ring structure followed by the assembly of proteins for axial structures, each of which is secreted by the flagellum-specific export apparatus (except FlgA, FlgI, and FlgH).

the cytoplasmic face of MS ring (Francis *et al.*, 1994). The C ring contains mostly two switch proteins FliM and FliN (Zhao *et al.*, 1996a,b), and is associated with MS ring via another switch/motor protein FliG, which probably contributes to a part of the face of MS ring (Thomas *et al.*, 2006). Assembly of these three proteins on the basal body requires the MS–ring platform, and mutations give rise to the nonflagellate phenotype. Inside the MS ring, there is the flagellum–specific export apparatus, visualized in freeze–fracture images as a protrusion inside the C ring (Katayama *et al.*, 1996). When the export apparatus is established in the flagellar base is still unclear. Details of the export apparatus are described in Section 2.2.

After the export apparatus is constructed, structural proteins for the basal body, expressed from class 2 operons, are secreted through the export apparatus in the order described below. First, the proximal rod, composed of FlgB, FlgC, and FlgF, is added on the MS ring, probably in this order (Homma *et al.*, 1990). FliE is needed for this assembly, joining FliF, and proximal rod as an adaptor (Minamino *et al.*, 2000b). Then the distal rod, made of FlgG, is assembled on the proximal rod. Formation of the rod requires FlgJ, which is exported to the periplasmic space via export apparatus and acts as a cap on the growing rod to facilitate the polymerization at the tip (Kubori *et al.*, 1992). FlgJ also has a muramidase activity at its C-terminal half, hydrolyzing the peptidoglycan adjacent to the MS ring to allow the rod to penetrate the peptidoglycan layer (Nambu *et al.*, 1999). Then the P ring (made of FlgI) is formed around the distal rod, followed by L-ring (FlgH) formation (Chevance *et al.*, 2007). FlgI and FlgH are not secreted through the export apparatus, but through the Sec pathway using a signal sequence at their N-termini (Homma *et al.*, 1987). P-ring formation requires the Dsb system, which is involved in intramolecular disulfide bond formation in the periplasm (Dailey and Berg, 1993). FlgI protein contains two cysteine residues important for protein stability (Hizukuri *et al.*, 2006). P-ring formation also requires the FlgA protein that acts as a periplasmic chaperone, assisting a polymerization reaction of FlgI into the P ring through FlgI–FlgI interaction (Nambu and Kutsukake, 2000). The hook assembles next, from about 120 copies of FlgE proteins at the distal end of the growing hook, with the aid of hook-capping protein FlgD. Hook elongation proceeds to the well-controlled length of 55 ± 6 nm by a sophisticated export switching mechanism (Hirano *et al.*, 1994). After hook reached to the defined length, FlgD dissociates from the tip of the hook, then replaced by the three HAPs, FlgK, FlgL, and FliD in this order (Homma and Iino, 1985). Addition of FlgK and FlgL is facilitated by the chaperone FlgN (Fraser *et al.*, 1999), whereas that of FliD is facilitated by another chaperone FliT (Bennett *et al.*, 2001). Finally, the FliC filament subunits (flagellin) are inserted at the distal end (Iino, 1969). FliD acts as a cap to facilitate the filament elongation by inserting each FliC subunit between the FlgL and FliD zones, with rotary cap mechanism revealed by

electron cryomicroscopic observation (Yonekura *et al.*, 2000). Mutants that lack FliD cannot polymerize the filament and excrete flagellin monomers into the culture (Homma *et al.*, 1984). However, when purified FliD is added to this mutant, flagellins stop leaking out and start polymerizing on the hook (Homma *et al.*, 1986). Using this system, growth rate of the filament was observed and revealed that initial growth rate is about 30 nm/min, which corresponds to one flagellin incorporated per second, suggesting that to reach the 10 μm long of the filament of wild-type cells, it takes several generations (Ikeda *et al.*, 1993).

  Vibrio alginolyticus has a single polar flagellum, so components required for polar flagellum are localized to a single cell pole. The mechanism for directing the MS ring (or to initiate MS-ring assembly) at the pole has remained unknown, but recent studies revealed that two proteins, FlhF and FlhG, are somehow involved in the process (Kusumoto *et al.*, 2006). Almost all of the cells of an *flhF* null strain do not have a polar flagellum, whereas an *flhG* strain has multiple flagella at a pole. Overproduction of FlhF in the wild-type strain increased the number of polar flagella, whereas excess FlhG reduced it, indicating that these two proteins function in opposing ways. Although the *flhFG* double null strain also showed almost no flagella, a very small but significant fraction of the cells possesses several flagella at the lateral position (Kusumoto *et al.*, 2008). These results suggest that FlhF functions in polar location of the flagellum. This idea is supported by a study in *Pseudomonas putida*, possessing polar flagella, which showed that an *flhF* mutant exhibits a peritrichously flagellated phenotype (Pandza *et al.*, 2000).

  FlhF and FlhG show similarity to FtsY and MinD, respectively. FtsY is a component of the prokaryotic SRP receptor (Luirink and Sinning, 2004) and MinD is a cell division inhibitor (Shapiro *et al.*, 2002). MinD shows a structural similarity to Ffh (Cordell and Lowe, 2001), which is a prokaryotic SRP that forms a complex with FtsY to function in a signal recognition targeting pathway for protein secretion at the membrane (Focia *et al.*, 2004). Therefore, FlhF may function together with FlhG in the same manner with FtsY/Ffh system to locate flagellar components, possibly the MS-ring protein FliF, to the cell pole. The direct interaction between FlhF and FlhG has been suggested (Kusumoto *et al.*, 2008). A recently reported crystal structure of FlhF from *Bacillus subtilis* revealed a dimer formation of FlhF and significant structural similarity of FlhF to FtsY/Ffh, supporting the idea described above (Bange *et al.*, 2007). However, many features of the polar localization mechanism remain unknown.

1.4. Regulation of rotation

Most flagellar motors are reversible rotary machines, able to rotate both clockwise (CW) and counterclockwise (CCW) (Silverman and Simon, 1974). Rotational switching completes very quickly, within only 1 ms

(Kudo *et al.*, 1990). Rotational direction is controlled by environmental stimuli, such as pH, temperature, and chemicals like sugars and amino acids. Methyl–accepting chemotaxis proteins (MCPs) sense these stimuli and transmit signals to the motor through a two-component phosphorelay signaling cascade (Fig. 2.5). When a repellent signal is sensed by the MCP, autophosphorylation activity of the CheA protein, associated with MCP on the cytoplasmic side, is activated and a histidine residue of CheA is phosphorylated. Then this phospho group is transferred to the Asp residue of the response regulator CheY. Phosphorylated CheY protein (CheY-P) then associated with the motor to trigger CW rotation. On the other hand, when an attractant signal is sensed by the MCP, autophosphorylation activity of CheA is repressed, so that the level of CheY-P decreases and the motor rotates in its default direction, CCW. The molecular mechanisms of MCP function and two-component signaling are reviewed elsewhere (Armitage, 1999; Parkinson *et al.*, 2005).

The target of CheY-P in the motor is the switch complex, composed of FliG, FliM, and FliN. As described above, FliG/FliM/FliN complex is also called ''the switch complex'' because mutations in these proteins cause defects in switching the CCW/CW rotation in response to tactic stimuli. FliM functions most directly in regulation of the switching frequency by binding to CheY-P (Welch *et al.*, 1993). This binding of CheY-P to FliM probably changes the FliG–FliM interaction, and causes movement of the C-terminal domain of FliG (FliG$_C$) that interacts with the stator protein MotA, thereby altering the rotor–stator interface to switch the direction of rotary motion.
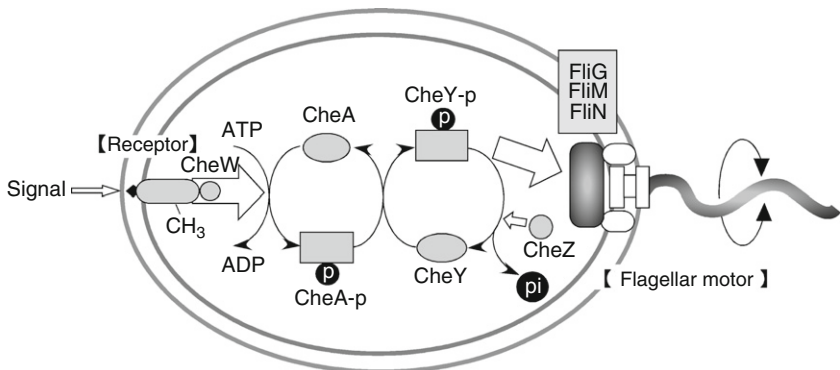
Figure 2.5 Schematic diagram of signal transduction of *Escherichia coli* chemotaxis. The chemoreceptors are embedded in the cytoplasmic membrane and localized at a pole. Chemotaxis substances or ligands bind to the receptor and the signals are transmitted into a cell and are transferred through the two-component phosphorelay system via the Che proteins. The phosphorylated CheY can bind to FliM and the direction of the motor rotation is changed.

Studies of intracellular level of CheY–P in a single cell that causes switching from CCW to CW revealed that switching is a highly cooperative event, showing a Hill coefficient of about 10, suggesting that chemotactic signal is amplified within the switch (Cluzel *et al.*, 2000). Fluorescence resonance energy transfer-based observation of CheY interaction with FliM by using CFP-FliM and CheY-YFP showed that binding of CheY–P to FliM is much less cooperative than motor switching (Hill coefficient of 1.7 ± 0.3) (Sourjik and Berg, 2002). This result was further supported by *in vitro* biochemical studies showing that CheY–P binding to the isolated intact switch complex was not cooperative (Hill coefficient is around 1) (Sagi *et al.*, 2003). These results indicate that the chemotactic signal is amplified within the switch, but subsequent to the CheY–P binding to FliM.

Some bacteria respond to tactic stimuli using modes, other than directional switching. *Rhodobacter sphaeroides* has a unidirectional flagellar motor that alternates between CW rotation and brief stops, during which the bacterium is reoriented by Brownian motion and changes in flagellar filament morphology (Armitage and Macnab, 1987). In the case of *Sinorhizobium meliloti*, the motor also rotates unidirectionally in the CW direction and swimming cells respond to tactic stimuli by modulating the flagellar rotary speed (Schmitt, 2002). The marine bacterium *V. alginolyticus* has dual flagellar systems, Na^+–driven polar flagellum (Pof) and H^+–driven lateral flagella (Laf), and their switching modes are different: the Laf motor rotates unidirectionally in CCW and responds to tactic signals by slowing down, whereas the Pof motor turns in both directions (Kojima *et al.*, 2007). In each case described, tactic signals are transmitted through the two–component signaling pathway, and CheY–P association to the motor modulates rotation.

2. BASAL STRUCTURE OF FLAGELLA AS MOTOR

2.1. Basal body

Structural features and the components of the basal body are described in Section 1.1. The supramolecular complex of the basal body is constructed by 7 kinds of proteins and ~130 molecules in total are assembled (Macnab, 2003). Aizawa *et al.* (1985) established a method to isolate the basal body of *Salmonella* with high yield and purity. Using this method, but greatly modified to allow C–ring isolation, the structure of the flagellar basal body and C ring of *Salmonella* had been investigated by the single particle analysis using negatively stained– or cryo-electron microscopy (Francis *et al.*, 1994). A resolution was obtained at 20 Å that is used for building the three-dimensional reconstitution

of images (Suzuki *et al.*, 2004; Thomas *et al.*, 2001, 2006). The flagellar basal body has a rotational symmetry with its axis in the center of the rod. The center of the rod is a hollow tube and the flagellar components required for axial structure are exported through this tube. The detailed single particle analysis of the MS ring revealed an interface between the MS ring and rod (Suzuki *et al.*, 2004). The MS ring looks like a cylinder mounted on two disks. Suzuki *et al.* (2004) reported that the MS-ring structure can be divided into five domains (C, P, S, M, and R), and discussed functions of each domain. The near-axial C and P domains are involved in the protein export and thought to change its conformation by the association with the export apparatus and open a channel through the protein. The C domain associates with the most proximal side of the rod and thereby the rod begins its assembly on the C domain. Although the S and M domains form the two disks characteristic of the MS ring, their functions are not clear. The R domain that forms cylinder-like part attaches to the outer face of the rod. It was speculated that the interaction between the rod and R domain is important for the rod–MS ring junction to release the twisting stress and symmetry mismatch. Thomas *et al.* (2006) has greatly improved resolution of images, by classifying particles according to size and applying the averaging procedures appropriate for each symmetry class. This improvement allows us to see for the first time the detailed feature of the C ring, not just a dumbbell-like structure. Their images revealed that the symmetry of individual M rings varies from 24-fold to 26-folds, whereas that of the C rings varies from 32-fold to 36-fold, with no apparent correlations between the symmetries of the two rings. The resolution of these improved EM images is now good enough to allow the crystal structures solved for the C-ring components to be docked into the map. The LP ring is an extraordinarily rigid structure and can maintain the ring morphology even under stringent condition such as 7.5 M urea (Akiba *et al.*, 1991). Single particle analysis revealed that the P ring looks like a dumbbell and seems to contact with a part of the rod, whereas the L ring seems not to contact the rod (Stallmeyer *et al.*, 1989).

MotX and MotY, which are required for the rotation of the polar flagellar motor of *V. alginolyticus*, are associated with the basal body and form an additional ring structure beneath the LP ring, termed T ring (Terashima *et al.*, 2006). Partial T-ring structures were observed in the ΔmotX strain but not in the ΔmotY and ΔmotXΔmotY strains, suggesting that MotX associates with the basal body via MotY to form a complete T-ring structure. Stoichiometry of the MotX and MotY proteins in the T ring has not been determined yet. Further detailed observations of the T ring to reconstruct the three-dimensional images will be informative to understand their function.

2.2. Export apparatus

Most of the flagellar substructures are constructed beyond the cytoplasmic membrane. Therefore, protein components, synthesized in the cytoplasm, must be exported across the inner and outer membranes to be assembled at the appropriate final destinations. This is achieved by the flagellum-specific export apparatus that resides inside the MS-ring structure (Macnab, 2004). This system has a character in common with the needle complex that works for the secretion of virulence factors by pathogenic bacteria (Cornelis, 2006). Morphology of these two secretion machineries is quite similar to each other, and they are now classified in the type III export pathway (Hueck, 1998). The flagellum-specific export apparatus exports protein substrate in order without signal peptide cleavage. Most of the studies for the export apparatus have been carried out in *Salmonella*, and here we describe its general overview.

The core of the export apparatus is composed of six transmembrane proteins, FlhA, FlhB, FliO, FliP, FliQ, and FliR, that form an export channel complex inside the MS-ring structure. Three cytosolic proteins FliH, FliI, and FliJ are required for flagellum-specific export and interact with the channel, thereby contributing a part of the export apparatus. Recent study revealed that flagellar C-ring protein FliN is also involved in the export, so it is a part of the apparatus (Brown *et al.*, 2005; Gonzalez-Pedrajo *et al.*, 2006; McMurry *et al.*, 2006; Paul *et al.*, 2006). FlhA and FlhB have a large cytoplasmic domain at their C-termini, where soluble components interact with. The export apparatus (or a part of it) has been visualized as a protrusion inside the C ring, by the freeze-fracture image (Katayama *et al.*, 1996). However, only FliP and FliR have been detected in the basal body preparations so far (Fan *et al.*, 1997). FliI is an ATPase and its sequence shows similarity to the β subunit of the $F_O F_1$-ATPase, a rotary motor that drives chemical reaction of ATP synthesis (Fan and Macnab, 1996). Recently, crystal structure of FliI is solved at 2.4 Å, and revealed that its similarity is not only in the sequence (29% identity) but also in the structural level (Imada *et al.*, 2007). FliI is a member of the Walker-type ATPase family, and it is thought to form a ring-shaped hexamer for protein export (Claret *et al.*, 2003; Minamino *et al.*, 2006). These lines of evidence lead to an attractive model that FliI hexamer functions as a motor, unfolding and threading export substrates thought its central channel by cooperative conformational changes of subunits, just as speculated for AAA ATPase complexes. ATPase activity of FliI is negatively regulated by binding to FliH, in a complex of $FliH_2 FliI_1$ stoichiometry (Minamino and Macnab, 2000a). FliH also binds to the hydrophobic patch of FliN, and their interaction would mediate efficient localization of FliI near the C-ring complex. FliJ is a general chaperone, preventing aggregation of export substrates presumably by interacting with them (Fraser *et al.*, 2003;

Minamino *et al.*, 2000a). Interactions among export components have been investigated by far-western method (affinity blotting), and it was found that cytosolic components interact with each other and probably forming FliH/FliI/FliJ complex in some point, and the cytoplasmic domain of membrane components FlhA and FlhB interacts with all soluble components (Minamino and Macnab, 2000b). Affinity blotting experiments also indicate that cytoplasmic domain of FlhA and FlhB interact with substrates, suggesting that these two proteins are involved in protein translocation. From these results, the outline of export is emerging: protein substrate is captured by FliH/FliI/FliJ complex without denaturation and transferred to the export apparatus. In the same time, FliI docks to the cytoplasmic face of the apparatus, forming hexameric ring structure that has an enhanced ATPase activity released from FliH inhibition. Then the substrates are exported through a central channel of apparatus, probably formed mainly by transmembrane segments (TMs) of FlhA and FlhB. After crossing the inner membrane, substrates are assembled at the appropriate position in ordered fashion, from the innermost structure to the external ones.

   How is this ordered export achieved? As discussed in Section 1.2, coupling of flagellar gene expression to the stages of flagellar assembly makes it possible for the ordered export. But there is one more mechanism operating in the flagellum–specific export apparatus: the substrate-specificity switching (Kutsukake *et al.*, 1994). The apparatus has two export substrate-specificity states, the rod/hook type and the filament type (Minamino and Macnab, 1999). Therefore, proteins forming the rod and hook structures are exported prior to the proteins required for filament formation. When the hook structure reaches a certain length (ca 55 nm), FliK and FlhB sense this state, and the substrate specificity of the apparatus switches from the rod/hook type to the filament type, causing the export of a new substrate class (Ferris and Minamino, 2006; Moriya *et al.*, 2006; Shibata *et al.*, 2007; Waters *et al.*, 2007). In addition, this switching leads to FlgM export, followed by expression of the class 3 operons (Hughes *et al.*, 1993; Kutsukake, 1994). It is reported that this switching is irreversible (Minamino *et al.*, 1999).

2.3. Switch complex

The switch complex functions in the rotation/switching/assembly of the flagellum and is composed of the three kinds of proteins, FliG, FliM, and FliN (Fig. 2.6). Null mutants of each protein exhibit Fla$^-$ phenotype (non-flagellate), and point mutations give rise to Fla$^-$, Che$^-$ (defective in chemotaxis), and Mot$^-$ (defective in motility) phenotypes (Yamaguchi *et al.*, 1986a, b). Stoichiometry of the FliG, FliM, and FliN in the C ring have been reported to be 26, 34, and more than 100 copies, respectively (Francis *et al.*, 1992; Suzuki *et al.*, 2004; Thomas *et al.*, 1999). Three-dimensional
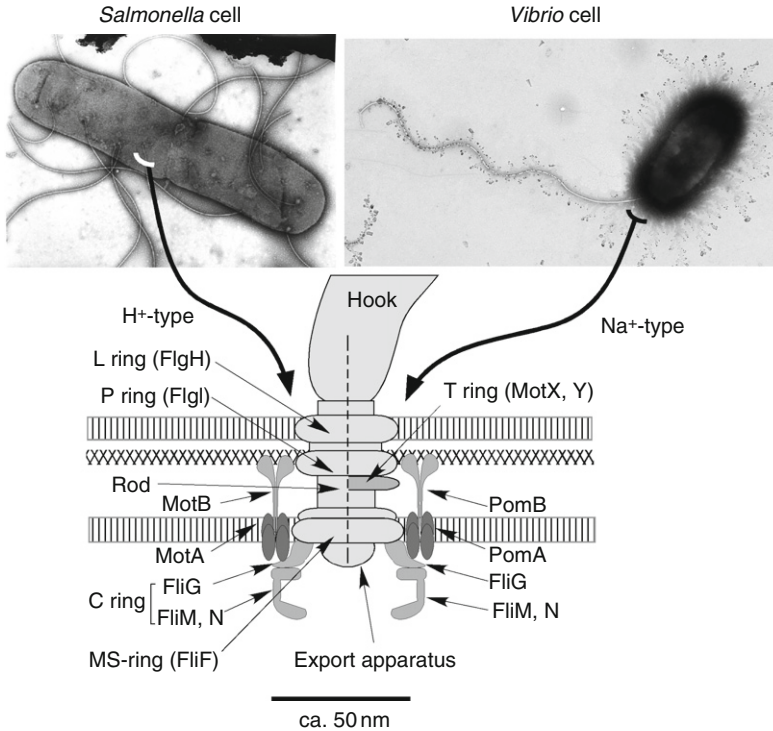
Figure 2.6   Cell body and flagellar basal structure of the proton- and sodium-driven type. The components emphasized by darker drawing are essential components for torque generation. The stator of flagellar motor consists of MotA and MotB of H^+-driven motor in *Escherichia coli* and of PomA and PomB of Na^+-driven motor in *Vibrio alginolyticus*. For the Na^+-driven motor, additional components of MotX and MotY, which form a T ring in the basal body, are also essential. Ion flow through MotAB or PomAB complex is believed to be coupled with torque generation by the interaction between the stator component of MotA or PomA and the rotor component of FliG. Electron micrograph of osmotically shocked *Salmonella* cell to visualize flagellar base is shown in left photograph. The flagellum of *V. alginolyticus* cell is observed and visualized by the electron microscopy in right photograph.

reconstructions from electron cryomicrographs of the rotor revealed that the C ring displays ∼34-fold symmetry and the MS ring shows about 25-fold symmetry (Thomas *et al.*, 2006), and confirmed that most of the C-ring structure was composed of FliM and FliN. It was known that the FliF binds to FliG, and N-terminal 46 residues of FliG are required for the binding (Oosawa *et al.*, 1994). Recent studies revealed more detailed FliG–FliM interactions, and it will be discussed later (Brown *et al.*, 2007). In addition, spontaneous mutants of FliF–FliG fusion were found to be functional (Francis *et al.*, 1992). Therefore, the FliF:FliG ratio should be 1:1, and it is

consistent with FliG stoichiometry in C ring and the symmetry of MS ring as described earlier. By direct comparison of the ring structure made of FliF and FliF–FliG fusion protein obtained by electron cryomicroscopy and single-particle image revealed that a part of the FliG occupies the outer rim and face of the M ring, whereas the remaining part is likely a part of the C ring (Suzuki et al., 2004). FliM interacts with FliG and FliN but not with FliF, and FliN does not interact with FliF (Oosawa et al., 1994). Therefore, FliM and FliN are probably located at the central and bottom position of the C ring, respectively.

Structural studies of the switch proteins have been undertaken by using the thermophilic bacteria *Thermotoga maritima* as a protein source, and crystal structures of the functional domains have been determined (Fig. 2.7). For FliG, middle and C-terminal domains of the protein (residues 104–335, termed $FliG_{MC}$) correspond to two-third of the full-length protein (Brown et al., 2002; Lloyd et al., 1999). The middle domain (residues 115–190, termed $FliG_M$) has a conserved surface patch formed by the residues $EHPQ_{125–128}$ and R_{160} (the EHPQR motif), which is important for binding to FliM (Brown et al., 2007). The $FliG_C$ (residues 198–335) has a conserved surface hydrophobic patch, which is also important for the binding to FliM (Brown et al., 2007). A region near the C-terminus has five well-conserved charged residues that interact with those in the stator protein MotA, and electrostatic interaction of these charged residues at the rotor–stator interface is important for torque generation (Lloyd and Blair, 1997; Zhou et al., 1998a). Structure showed that charged residues of FliG are clustered on the prominent ridge of $FliG_C$ where two subsets of the charged residues are aligned as a ''V''-like shape. $FliG_M$ is connected to the $FliG_C$ by an α-helix and short linker including well-conserved two consecutive Gly residues (termed Gly–Gly motif). This Gly–Gly motif seems to be involved in the motion of both domains, acting as a flexible hinge mediating relative movements of two connecting domains. These structural features of FliG suggest that FliG is likely to have two orientations that bring different subset of charged residues into alignment around the edge of the rotor, where they could interact sequentially with charged residues of the stator protein MotA. Therefore, such an arrangement of charged residues may be important for the switching of the rotational direction. Yeast two–hybrid method was used to investigate the interaction between switch proteins, and revealed two distinct binding sites for FliM in FliG: the EHPQR motif of the $FliG_M$ and the hydrophobic patch of the $FliG_C$ (Marykwas et al., 1996). Consistent with this, tryptophan replacements in residues that participate in these binding sites influenced the binding to FliM and also the assembly of the flagellum (Brown et al., 2007). The hydrophobic patch in $FliG_C$ is positioned adjacent to the Gly–Gly linker and opposite to charge-bearing ridge. Because the structure of the N-terminal domain has not been determined yet, it is not clear how FliG binds to FliF.
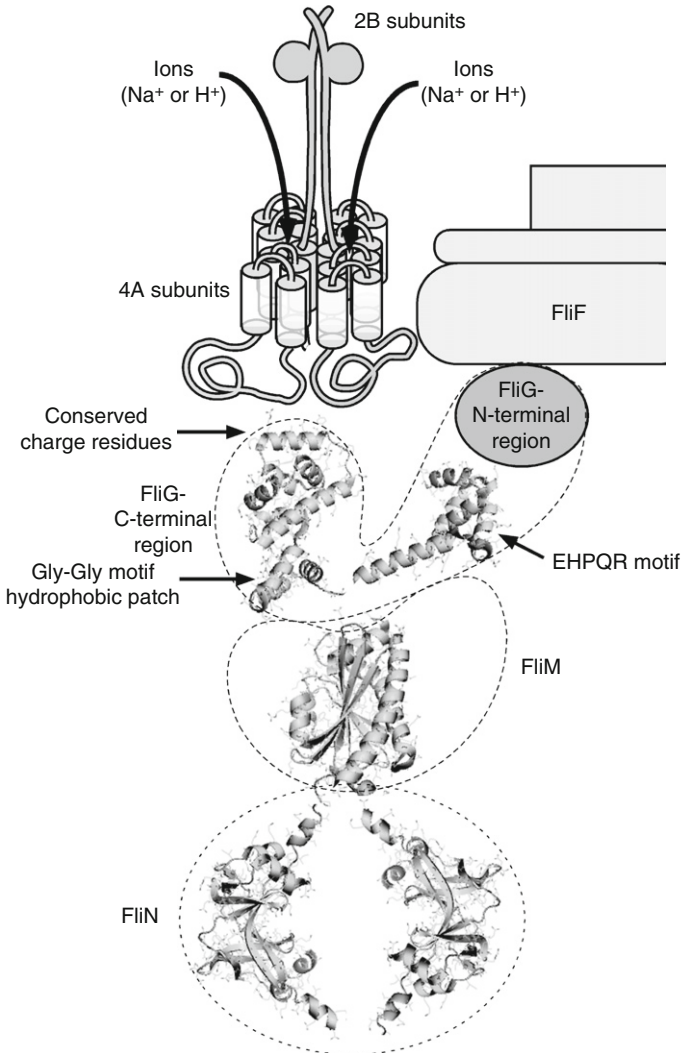
Figure 2.7   The structures of stator and rotor. The stator is formed by the MotA$_4$MotB$_2$ or PomA$_4$PomB$_2$ complex. The B subunit has a peptidoglycan-binding motif (protruded ball) and the A subunit has large cytoplasmic domain, containing the conserved charged residues important for flagellar rotation, between second and third transmembrane segments. The crystal structure of the FliG middle and the C-terminal domain, the FliM middle domain, and the two-third of FliN of *Thermatoga maritima* are shown using the PDB data, 1l kv, 2hp7, and 1yab, respectively. The C-terminal region of FliG has a ridge containing the important charged residues, which are believed to interact with the charged residues of the cytoplasmic domain of MotA, for the flagellar rotation. FliN is depicted as a homotetramer composed of dimer–of–dimers. FliG, FliM, and FliN form a switch complex. FliF forms the MS ring of the basal body.

However, as noted above, since FliF–FliG fusion protein is functional, the C-terminal end of FliF and N-terminal end of FliG are likely to be in proximity.

Crystal structure of the middle domain of FliM (residues 44–226, termed FliM$_M$) from *T. maritima*, which corresponds to two-third of the full-length protein, has been determined (Park *et al.*, 2006) (Fig. 2.7). FliM is involved in changing of the rotational direction triggered by the binding of CheY-P to FliM, a chemotactic signaling molecule (Sockett *et al.*, 1992; Welch *et al.*, 1993). The phosphorylation state of CheY is regulated by a kinase (CheA) and phosphatase (CheZ, CheC, or CheX), which are involved in chemotactic signaling pathway (Parkinson, 2003). The structure of FliM reveals structural similarity to these phosphatases. Disulfide cross-linking experiments using Cys-substituted FliM variants designed by using the structural information revealed the interface of FliM protein responsible for its self-association in the C-ring structure. Based on this arrangement of FliM subunits, about 33–35 copies of FliM subunits form a ring with a diameter of ∼44 nm, consistent with its rotational symmetry (34-fold) in the C ring observed in electron cryomicroscopy (Thomas *et al.*, 2006, 1999). CheY-P binds to N-terminal portion of FliM, which is not present in the structure. Truncation of the N-terminal 43 residues is required for crystal growth of FliM$_M$. It is probably disordered when extracted from the C-ring structure. On the other hand, crystal structure of CheY protein in complex with FliM peptide including N-terminal 16 residues has been reported (Dyer and Dahlquist, 2006; Lee *et al.*, 2001). The CheY-FliM peptide structure revealed the allosteric communication between the phosphorylation site and the target-binding surface of CheY protein. The C-terminal part of FliM has been shown to be important for the binding to FliN (Marykwas *et al.*, 1996). A GGXG motif involved in the interaction with FliG exists in the opposite side of the FliN–binding region (Mathews *et al.*, 1998; Tang *et al.*, 1996; Toker and Macnab, 1997). However, weak electron density in this region discerns only the first two glycine residues.

The structure of FliN corresponding to the two-third of full-length protein (residues 68–154) from *T. maritima* (Brown *et al.*, 2005) has been determined. FliN, that mostly contributes to form the C-ring structure, is found to be a tightly intertwisted dimer composed mostly of β-sheet (Fig. 2.7). Structure also revealed a hydrophobic patch, formed by several well-conserved hydrophobic residues, on the surface of the FliN dimer. Mutations in these residues in the patch give rise to Fla$^-$ or Che$^-$ phenotype, indicating that it is important for the flagellar assembly and the switching. Motility of these mutants is partially restored by the overexpression of FliI and FliH (Paul *et al.*, 2006), soluble components of export apparatus, suggesting that FliN is involved in the secretion of flagellar proteins. This is not surprising, since a temperature-sensitive FliN mutant was unable to regrow flagellar filament after shearing it at the restrictive temperature

(Vogler *et al.*, 1991). FliN has been known to involve the export of filament subunits or capping proteins. In addition, FliN has a homology to the export apparatus for virulence factors of pathogenic bacteria (Tang *et al.*, 1995). Therefore, although FliN is involved in switching and motility, it is more directly involved in flagellar assembly, probably as a part of flagellum-specific export apparatus. Consistent with this idea, recent biochemical studies showed that FliN associates with FliH (McMurry *et al.*, 2006; Paul *et al.*, 2006), and a five-protein complex consisting of FliG, FliM, FliN, FliH, and FliI can be isolated (Gonzalez-Pedrajo *et al.*, 2006). These lines of evidence suggest that FliN in C ring provides a docking site for export substrate via FliH to efficiently deliver them to the apparatus, and FliN–FliH interaction involves the hydrophobic patch of FliN. Contribution of FliN to the rotational switching is also involved in the hydrophobic patch. Mutations giving Che$^-$ phenotype are mapped around the hydrophobic patch, and defects could be partially rescued by overexpression of the CheY, suggesting that FliN may contribute to the binding site of CheY-P (Paul *et al.*, 2006). As describe earlier, FliN occupies most part of the C ring, and it is located at the bottom of the ring. Analytical ultracentrifugation of purified FliN of *T. maritima* showed that the FliN exists as a dimer in solution, and FliM and FliN together form the stable $FliM_1/FliN_4$ complex (Brown *et al.*, 2005). *E. coli* FliN exists as a stable homotetramer in solution. These results are consistent with the stoichiometry of FliM to FliN in the C ring. Targeted disulfide cross-linking studies of FliN suggested that FliN is organized in doughnut-shaped tetramers, whose shape is closely matched for the bottom of C ring in the reconstructed electron microscopic image (Paul and Blair, 2006).

2.4. Motor complex

The MotA/MotB or PomA/PomB complex that acts as the torque-generating unit exists in the cytoplasmic membrane and assembles around the rotor (Kojima and Blair, 2004a; Yorimitsu and Homma, 2001). MotA and MotB form the torque-generating unit of the H^+-driven flagellar motor, whereas PomA and PomB form that of the Na^+-driven flagellar motor of *Vibrio* spp. and are orthologues of MotA and MotB (Asai *et al.*, 1997; Dean *et al.*, 1984; Stader *et al.*, 1986) (Figs. 2.7 and 2.8). MotA and PomA have four TMs (Asai *et al.*, 1997; Zhou *et al.*, 1995). A large cytoplasmic loop between the second and third TMs contains conserved charged residues that have been shown to interact with the conserved charged residues in the rotor protein FliG, and their electrostatic interactions are important for torque generation (discussed also in Section 3.1; Lloyd and Blair, 1997; Zhou and Blair, 1997; Zhou *et al.*, 1998a) (Fig. 2.8). On the other hand, periplasmic loops between first and second TMs (loop1–2) and third and fourth TMs (loop3–4) are very short. MotB and
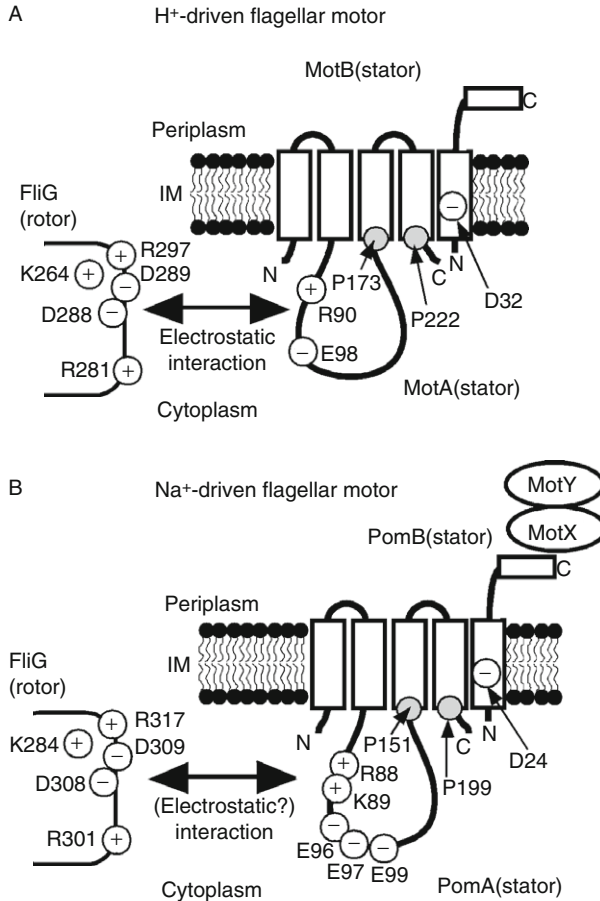
Figure 2.8 Charged residues of the putative interaction surface between stator and rotor. The *Vibrio alginolyticus* PomA R88 and E96 correspond to R90 and E98 of the *Escherichia coli* MotA, and K284, R301, D308, D309, and R317 of *V. alginolyticus* FliG correspond to K264, R281, D288, D289, and R297 of *E. coli* FliG, respectively. The aspartic acid residue in B subunit (D32 in MotB and D24 in PomB) is believed to be an ion-binding site.

PomB have a single TM at its N-terminus (Asai *et al.*, 1997; Chun and Parkinson, 1988). This TM contains an absolutely conserved negatively charged residue (Asp32 in MotB of *E. coli* and Asp24 in PomB of *V. alginolyticus*), which is critical for motor rotation and predicted to be the ion-binding site in the stator complex (Zhou *et al.*, 1998b). Most of MotB and PomB proteins are located in the periplasmic space. C-terminal portions of MotB and PomB contain the putative peptidoglycan-binding (PGB) motif that is well conserved among proteins such as OmpA and Pal,

which are outer membrane proteins that interact with the peptidoglycan layer noncovalently (De Mot and Vanderleyden, 1994; Koebnik, 1995). The MotA/MotB and PomA/PomB complexes are also called the stator, the nonrotating part of the motor. The stator complex forms a heterohex-amer composed of four A subunits (MotA or PomA) and two B subunits (MotB or PomB) (Kojima and Blair, 2004b; Sato and Homma, 2000a,b; Yorimitsu *et al.*, 2004). The MotA/MotB stator functions as a H^+ channel and the PomA/PomB stator functions as an Na^+ channel (Blair and Berg, 1990; Sato and Homma, 2000a; Stolz and Berg, 1991).

Although structural information is critical to understand the mechanism for torque generation, currently there are no high-resolution structural data on the stator complex because its strongly hydrophobic nature hinders to obtain crystals. Instead, arrangements of the TMs of MotA and MotB from *E. coli* (18 segments total in a complex) have been investigated by systematic disulfide cross-linking studies. The results uncovered initial picture of the MotA/MotB stator complex: a symmetric dimer of MotB segments is at the center of the complex, and TMs of four MotA molecules are arranged around the MotB dimer (Braun and Blair, 2001; Braun *et al.*, 2004). Cys residues introduced in the third and fourth TMs (TM3 and TM4) of MotA can form disulfide bridges between those introduced in the single TM of MotB that contains the proton-accepting Asp residue, suggesting that proton-conducting channel is formed by these three segments. Arrange-ment of the MotB dimer that fits to the cross-linking results revealed that the critical Asp32 residues of two MotB molecules are positioned on the separate surface of the MotB dimer, so possibly there exist two proton-conducting channels in a $MotA_4/MotB_2$ stator complex. This arrangement seems to fit into the PomA/PomB Na^+-conducting stator complex: the TM3 of PomA positions very near the TM of PomB (Yakushi *et al.*, 2004). Phenamil, a potent inhibitor for eukaryotic epithelial sodium channel, also specifically inhibits the rotation of Na^+-driven motor (Atsumi *et al.*, 1990). Mutations that allow motor to rotate in the presence of phenamil (Kojima *et al.*, 1997) were mapped near the cytoplasmic face of the TM3 of PomA (D148Y) and TM of PomB (P16S) (Jaques *et al.*, 1999; Kojima *et al.*, 1999), and when replaced to Cys, these two residues can form a disulfide bridge (Yakushi *et al.*, 2004). These results suggest that residues in TM3 of PomA and TM of PomB (including critical Asp24) may participate in forming an Na^+-binding site near the cytoplasmic face. Systematic Cys replacement of the residues located in the periplasmic loops of PomA revealed that Pro172, which locate in the loop3–4, forms cross-linked dimer under the oxidation condition, so loop3–4 of two PomA molecules are positioned side by side in a PomA/PomB complex (Yorimitsu *et al.*, 2000).

The number of the stator complexes assembled around the rotor was measured by various methods. The stepwise increase of the rotation speed that was dependent on the expression of the stator proteins (Blair and Berg,

1988; Block and Berg, 1984) and the fluorescence intensity change of green fluorescent protein (GFP)–MotB measured by fluorescence recovery after photobleaching (FRAP) method indicate that at least 11 stator complexes are estimated in a single motor (Leake *et al.*, 2006; Reid *et al.*, 2006). The electron cryotomography of whole cells of *Treponema primitia* showed *in situ* structure of the complete flagellar motor at the 7 nm resolution (Murphy *et al.*, 2006). The image indicates that the stator assembly possessed 16-fold rotational symmetry, within the range of the stator number described above. Recently, the purified PomA/PomB complexes reconstituted into the proteoliposome have been observed by cryo–electron microscopy and rough image of stator was reported (Yonekura *et al.*, 2006). Rod-shaped objects protruded out from both sides of the lipid bilayer. Its diameter was ~20 Å, and length of a longer rod and a shorter rod were ~70 and 35 Å, respectively. The PomA/PomB complex with truncated C-terminus of PomB, which lacks PGB motif, was also observed, and the longer rod is found to be the C-terminal domain that contains the PGB motif.

3. Torque Generation

In this chapter, we overview the current knowledge of the mechanism of torque generation, based on genetic and biochemical studies. Many hypotheses of torque generation have been proposed, and were extensively reviewed elsewhere (Berg, 2003; Kojima and Blair, 2004a). It is noteworthy that some interesting motor models were recently published (Schmitt, 2003; Xing *et al.*, 2006).

3.1. Interaction between stator and rotor

It is believed that the rotational force of the flagellar motor is generated by the interaction between the cytoplasmic loop region of the stator component, MotA or PomA, and the C-terminal domain of the rotor component, FliG. The rotor–stator interaction is coupled to the H^+ or Na^+ flow through the stator powered by the electrochemical gradient across the cytoplasmic membrane. Domains of MotA (or PomA) and FliG responsible for the rotor–stator interaction contain the conserved charged residues important for the torque generation (Fig. 2.8) (Lloyd and Blair, 1997; Yorimitsu *et al.*, 2002; Zhou and Blair, 1997). In *E. coli* motor, they were Arg90 and Glu98 of MotA, and Lys264, Arg281, Asp288, Asp289, and Arg297 of FliG (Fig. 2.8A). No single residue is critical for rotation, but they function collectively. Charge neutralization or inversion of these residues disrupts motor rotation, but certain combinations of MotA mutations with FliG mutations show strong synergism (e.g., MotA-R90A and

FliG R281A) or suppression (e.g., MotA–R90E and FliG D289K), which suggests that the charged residues of MotA interact with those of FliG (Zhou *et al.*, 1998a). Therefore, such electrostatic interactions between rotor and stator are important for the torque generation. As discussed in Section 2.3, crystal structure of the FliG$_C$ revealed that these charged residues are clustered on the prominent ridge of the FliG$_C$, where two subsets of the charged residues (R281/D288/K264 and R281/D289/R297) are aligned as a "V"-like shape (Lloyd *et al.*, 1999). Structure and genetic evidence lead to the rotational switching model that switching may result from distinct combination of electrostatic interactions between rotor and stator.

In the case of Na$^+$-driven motor of *V. alginolyticus*, these charged residues are also conserved in PomA and FliG (R88 and E96 of PomA and K284, R301, D308, D309, and R317 of FliG) (Fig. 2.8B). However, when these residues and neighboring additional three charges (K89, E97, and E99) of PomA were all neutralized, PomA was still functional (Yorimitsu *et al.*, 2002). Likewise, single or all possible combinations of charge–neutralizing mutations in five conserved charged residues did not affect the motility. Inversion of charge in PomA or FliG barely gave nonmotile or slow-motile phenotype (Yorimitsu *et al.*, 2002, 2003). These results suggest that Na$^+$-driven motor may require additional charged residues in PomA and/or FliG for complete electrostatic interaction(s). Alternatively, electrostatic interaction between rotor and stator are not important for the torque generation in *V. alginolyticus*. It was found that chimeric FliG protein consisting of the N-terminal two-third from *V. alginolyticus* and the C-terminal one-third from *E. coli* (termed FliG^{VE}) is functional in the *fliG* strain of *V. alginolyticus*, and its opposite variant of chimeric protein (N-terminal two-third from *E. coli* and C-terminal one-third from *V. alginolyticus*; FliG^{EV}) is functional in the *fliG* strain of *E. coli* (Yorimitsu *et al.*, 2003). Likewise, the MotA/MotB stator from *E. coli* is functional in the Δ*pomAB* strain of *V. alginolyticus* and its motor is driven by proton motive force (PMF) (Asai *et al.*, 2003). Chimeric protein PotB, consisted of the N-terminal TM of PomB from *V. alginolyticus* and the C-terminal periplasmic segment from *E. coli* MotB, is functional in the Δ*motAB* strain of *E. coli*, whose motor is driven by sodium motive force (Asai *et al.*, 2003) (Fig. 2.9A). These results indicate that certain parts of the motor responsible for rotation can be interchangeable between species, and general mechanism of the motor rotation is quite similar regardless of the coupling ion. To understand the role of charged residues in *V. alginolyticus* for motor rotation, conserved charged residues of *V. alginolyticus* with or without mutations were introduced into the hybrid *E. coli* motor composed of chimeric rotor (FliG^{EV}) and stator proteins (PomA/PotB), and Na$^+$–driven motility of the cells containing these motor proteins were investigated (Yakushi *et al.*, 2006). It was revealed that the charged residues in the
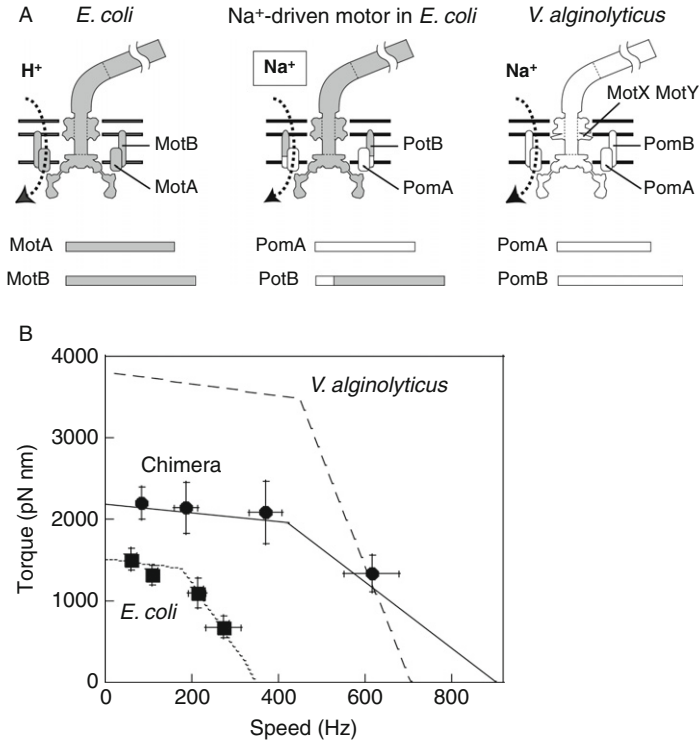
Figure 2.9 Hybrid and chimeric motors with the Na$^+$- and the H$^+$-driven components. (A) The gray and the open part show the regions of the H$^+$- (MotA or MotB) and the Na$^+$-driven components (PomA or PomB), respectively. The horizontal lines show the outer membrane, peptidoglycan layer, and the cytoplasmic membrane. (B) The torque–speed relationships of different flagellar motors. Measured speeds and estimated torques of chimeric motors are represented by circles, the H$^+$-driven *Escherichia coli* motor (squares) using filament drag coefficients (Inoue *et al.*, 2008). Dotted and dashed line are reported torque–speed relationships for H$^+$-driven *E. coli* motor (Chen and Berg, 2000b) and Na$^+$-driven *Vibrio alginolyticus* motor (Sowa *et al.*, 2003), respectively.

V. alginolyticus rotor and stator proteins were found to require for motor rotation when they were engineered in the *E. coli* motor, although the synergism and suppression in rotor–stator double mutants were weaker than those seen in *E. coli*. Therefore, basically rotor–stator interaction occurs in the *V. alginolyticus* motor in the same way as in *E. coli*, but the rotor–stator interface is more robust in *V. alginolyticus*. Additional charged residues of PomA may contribute such robustness (Obara *et al.*, 2008), but other factors, probably MotX and MotY, may enhance the motor function in *V. alginoltyticus*. The flagellar motor of *S. meliloti* rotates only CW direction, and its speed was modulated by the tactic stimuli (Gotz and Schmitt, 1987; Schmitt, 2002). Like *E. coli* and *V. alginolyticus*, electrostatic interactions

between conserved charged residues in rotor (R294 and E302 of FliG) and stator (R90, E98, and E150 of MotA) of *Sinorhizobium* are important for torque generation. Initially, it was expected that different charge distribution at the rotor–stator interface, due to the absence of several conserved charged residues in FliG (only two are conserved), might be the basis for the different modes of motor rotation. However, mutational analyses revealed that unlike *E. coli*, E150 is essential for torque generation, whereas R90 and E98 are crucial for chemotaxis-controlled modulation of rotation speed (Attmannspacher *et al.*, 2005). Therefore, it was proposed that MotA E150 interacts with FliG R294 to achieve fast rotation, but conformational changes in FliG triggered by CheY-P binding to FliM lead to the a new rotor–stator alignment that places E150 of MotA adjacent to D302 of FliG, so that electric repulsion between them might result in lower torque and slower rotation.

Biochemical analysis of the interaction between stator and rotor has not proceeded as compared to the genetic analysis. Only a study has been reported so far that demonstrated MotA–FliG or MotA–FliM interactions by pull-down assay (Tang *et al.*, 1996). Then what is the nature of torque generation? Although the structure of the stator complex has not been solved and physical property of the stator complex have been still unclear, systematic mutational studies indicated that MotB Asp32 of *E. coli*, which exists in the single TM of MotB, is the only protonatable residue in the motor proteins responsible for the flagellar rotation, suggesting that protonation of this critical aspartate in the stator complex triggers conformational changes in the stator complex that drive rotor (Zhou *et al.*, 1998b). To test this idea, protease susceptibility of MotA in complex with MotB was examined, and it was revealed that replacement of the critical aspartate (Asp32) of MotB to asparagine or any other small neutral amino acid caused a conformational change in MotA, that could be detected as a change of protease susceptibility (Kojima and Blair, 2001). MotA conformation is also restricted by the well-conserved prolines located at the cytoplasmic face of TM3 and 4 (Pro173 and Pro222 in *E. coli*). In a way that disrupts α-helix, forming β-turn, proline greatly affects secondary and tertiary structures of the protein. Mutations in Pro173 and Pro222 abolished or severely impaired motility, and mutant proteins exhibit strong dominant-negative effect on motility. Therefore, these residues might regulate the conformation of the MotA/MotB complex and/or control conformational changes (Braun *et al.*, 1999; Zhou and Blair, 1997).

3.2. Ion-binding site

As discussed in Section 3.1, an ion-binding site of the stator channel has been believed to be MotB D32 in *E. coli* and PomB D24 in *V. alginolyticus* (Yorimitsu and Homma, 2001). H^+ or Na^+ associates with the negatively

charged side chain of the acidic amino acid in the stator, although pK_a of carboxyl group in these residues in the physiological condition has not been measured yet. As described in Section 3.1, when the conserved acidic or basic amino acid residues in MotA, MotB, FliG, FliM, and FliN, those of which are important for torque generation, were replaced to Ala, all the mutants except D32A of MotB still retained motility (Zhou et al., 1998b). Replacement of Asp at position 32 of MotB to various amino acids showed that all but glutamate at that position were nonfunctional. Therefore, D32 of MotB is likely to serve as the proton–binding site in the stator complex. Likewise, PomB D24 probably functions as the binding site for Na$^+$. It is noteworthy that an Na$^+$ binds to the functionally critical glutamate residue (E139) in the crystal of NtpK protein, the channel component of another Na$^+$-translocating rotary motor, V$_O$V$_1$-ATPase from Enterococcus hirae (Murata et al., 2005). Recently determined crystal structures of Na$^+$-coupled transporters revealed that not a single but several side chains including backbone carbonyl group(s) participate in forming an Na$^+$-binding site (Hunte et al., 2005; Yamashita et al., 2005). Therefore, in the case of a PomA/PomB complex, there still may exist additional residues involved in formation of an Na$^+$-binding site, possibly including D148 of PomA and P16 of PomB, those of which affect phenamil resistance when mutated. Also, it is possible that charged residues at the channel entrance or exit or the main chain carbonyl group(s) of the hydrophobic residues lining in the channel may play important roles for the selective ion influx (Kojima et al., 2000).

It has been known that cell growth and motility are still normal even if the MotA/MotB complex is overexpressed more than 50 times over the wild-type level, suggesting that overproduced complexes are inactive for proton traslocation (Wilson and Macnab, 1988, 1990). When the N-terminal 60 residues of MotB that includes its single TM was fused to the unrelated polypeptide, consisted of 50 residues encoded by a part of TetA (MotB60-TetA), its overproduction together with MotA impairs the cell growth (Stolz and Berg, 1991), and this growth impairment was abolished by the mutation in D32 of MotB (Zhou et al., 1998b). These results led to the proposal that a part of the complex (possibly the periplasmic domain of MotB) blocks proton flow through the MotA/MotB channel making it inactive. This model is supported by the mutational study demonstrating that a deletion of the segment just C-terminal to the TM of MotB (Δ51–70) or substitution of the residues in that region (I58, Y61, F62, and P52/P65) causes a strong growth impairment when overproduced (Hosking et al., 2006). Detailed analyses of this region brought a model that the segment (termed "plug") consists of an amphipathic α-helix and is inserted into the cell membrane parallel with its periplasmic face to interfere with channel formation. Interaction of a MotA/MotB complex with a flagellar basal body triggers movement of the plug from membrane and opening of the proton channel. Therefore, this plug may play a central role

in regulating the open–closed states of the stator channel to prevent premature proton flow.

3.3. Ion specificity

So far, two types of the motor classified by the coupling ion have been identified: the H^+–type and the Na^+–type. Most motile bacteria including *E. coli*, *S. typhimurium*, *B. subtilis*, *R. sphaeroides*, and *Pseudomonas aeruginosa* have H^+–driven motor and *V. alginolyticus* and alkalophilic *Bacillus* have Na^+–driven motor (Berry and Armitage, 1999; Doyle *et al.*, 2004; Imae and Atsumi, 1989; Yorimitsu and Homma, 2001). It seems that since *V. alginolyticus* lives in the sea where Na^+ is abundant, it may have evolved to acquire Na^+–conducting activity through the stator complex.

Which part of the stator proteins determines ion specificity? The H^+–driven stator of the *Rhodobacter sphearoides* is composed of MotA (RsMotA) and MotB (RsMotB), and RsMotA are found to be remarkably similar to the Na^+–driven stator of PomA from *V. alginolyticus* (Asai *et al.*, 1999; Shah and Sockett, 1995). Both of them are composed of 253 amino acids and their identity is more than 40% over their entire length. RsMotB has similarity only to the transmembrane region of PomB. When RsMotA was expressed in the *pomA* strain of *V. alginolyticus*, the motor was functional and driven by Na^+–motive force. On the other hand, expression of RsMotB together with RsMotA in the *pomB* strain of *V. alginolyticus*, cells are nonmotile (Asai *et al.*, 1999). Therefore, determinants of ion specificity of stator should exist in the PomB (and MotB). A series of chimeric proteins, consisting of N–terminal RsMotB and C–terminal PomB (termed MomB) (Asai *et al.*, 2000), was constructed. Some of the MomB constructs, whose entire TM was derived from RsMotB, functioned as Na^+–type stator when coexpressed with RsMotA in the $\Delta pomAB$ strain of *V. alginolyticus*. In this case, four proteins RsMotA, MomB, MotX, and MotY are involved in the Na^+–driven rotation. Interestingly, a MomB construct, whose junction is between F33 and V34 of PomB, functions better as Li^+–driven motor than as Na^+–driven motor. Later, it was found that a chimeric protein of PotB, a fusion of N–terminal TM of PomB and the C–terminal periplasmic segment of *E. coli* MotB, functions as an Na^+–type stator in *E. coli* only when coexpressed with PomA (Asai *et al.*, 2003). In this case, just two proteins PomA and PotB are required for Na^+–driven rotation (Fig. 2.9A). These lines of evidence indicate that cytoplasmic and transmembrane domains of PomA/PomB complex are sufficient for Na^+–driven motility, and periplasmic C–terminal part of B subunit (MotB or PomB) determines the requirement of MotX and MotY for function. Probably, the size of channel pore is varied in these chimeric stator complexes, altering the ion specificity. More precise descriptions of ion specificity in the stator will be provided by the high–resolution atomic model of the stator complex.

3.4. Assembly of functional motor

Whereas the assembly mechanism of the axial flagellar structure is now well understood (see Section 1.3), the mechanism of stator assembly is still not clear. Early experiments showed that controlled expression of *motA* or *motB* in their defective strains demonstrated stepwise restoration of the rotation rate with equal speed increment that saturated at eight steps, suggesting that eight independently functioning MotA/MotB stator units are incorporated into the wild-type motor (Blair and Berg, 1988; Block and Berg, 1984). Recent studies with higher resolution reported that as much as 11 stator units can be incorporated (Reid *et al.*, 2006). This number is in proximity to the observed particles that surround the rotor by freeze-fracture images (Khan *et al.*, 1988). MotB has a putative PGB motif that is well conserved among proteins such as OmpA and Pal, which are outer membrane proteins that interact with the peptidoglycan layer noncovalently (De Mot and Vanderleyden, 1994; Koebnik, 1995). The PGB motif of MotB is believed to associate with the peptidoglycan layer to anchor the MotA/MotB stator complex around the rotor. It is not clear how and when MotA/MotB stator complexes are targeted and anchored at the appropriate position around the rotor.

In *V. alginolyticus* and *V. parahaemolyticus*, MotX and MotY have been identified as essential components for the rotation of Na^+-driven polar flagellar motors (McCarter, 1994a,b; Okabe *et al.*, 2001; Okunishi *et al.*, 1996). As described in Section 2.1, they attach to the basal body to form a ring structure (termed T ring) that can be observed beneath the LP ring by electron microscopy (Terashima *et al.*, 2006). Biochemical studies have shown that MotX directly interacts with MotY, and affects membrane localization of the PomA/PomB complex and of the PomB alone, suggesting an interaction between MotX and PomB (Okabe *et al.*, 2005). In addition, when MotX or MotY is absent, GFP-fused PomA or GFP-fused PomB in complex with their partner subunit does not localize at the flagellated cell pole, suggesting that MotX and MotY in the T ring are involved in the incorporation of PomA/PomB complex into the flagellar motor (Terashima *et al.*, 2006). Like MotB and PomB, MotY possesses peptidoglycan–binding motif and a recently solved MotY structure showed remarkably similar structure to the Pal and RmpM (OmpA homologue), well–known peptidoglycan–binding protein (Kojima *et al.*, 2008). Detailed functions of MotX and MotY are still unclear, but they are speculated to be involved in ion specificity, or in extremely rapid rotation (1100 Hz) approximately four times faster than that of *E. coli* (300 Hz).

In *S. meliloti*, MotC and MotE have shown to be involved in the motility and regulation of the rotation speed of the flagllar motor (Eggenhofer *et al.*, 2004; Platzer *et al.*, 1997). MotC is the periplasmic protein and regulates the rotation speed by acting on MotB. MotE is the specific chaperone for MotC and controls the rotation speed indirectly by regulating amount of the

MotC proteins in periplasm. These proteins do not show similarity to MotX and MotY. In some bacteria, two kinds of stator might be assembled to a single flagellar base. *Pseudomonas aeruginosa*, which has a single polar flagellum, has dual sets of *motA* and *motB* genes, *motAB* and *motCD*, as well as another gene, *motY*. All these five genes contribute to H$^+$–driven motility (Doyle *et al.*, 2004). Function of MotA/MotB stator requires MotY, and these three proteins are important for the surface swarming. On the other hand, MotC/MotD does not require MotY for its function, and they are important for the swimming in liquid. Furthermore, noncognate pairs like MotA/MotD and MotB/MotC can work together to generate torque: mutants that contain *motA/motD* or *motB/motC* double mutations still retain motility. Therefore, *Pseudomonas* cells seem to choose two types of stators for motility depending on the surrounding environment (swimming or surface swarming) (Doyle *et al.*, 2004; Toutain *et al.*, 2005). Similarly, when swarming on the surface, *V. parahaemolyticus* as well as *V. alginolyticus* cells induced multiple lateral flagella that are driven by proton–type motor (Atsumi *et al.*, 1992; McCarter *et al.*, 1988). The stator for lateral flagellar motors contains LafT and LafU, orthologues of MotA and MotB, and somehow its function requires a second set of MotY, MotY$_L$ (Stewart and McCarter, 2003). The reason why MotY$_L$ is necessary for rotation of the lateral flagellar motor is not clear.

Another example is the motor of *B. subtilis*: it has an Na$^+$–driven MotP/MotS stator and a proton–driven MotA/MotB stator, but a single set of flagellar rotor proteins (Ito *et al.*, 2004). Like the hybrid stator of *P. aeruginosa*, hybrid stators like MotP/MotB and MotA/MotS are functional in *B. subtilis* and ion specificities of these motors depend on the B subunit (MotA/MotS for Na$^+$–type and MotP/MotB for H$^+$–type) (Ito *et al.*, 2005). These results are consistent with the observation of hybrid motors with chimeric proteins using stator proteins of *V. alginolyticus* and *R. sphaeroides*. Since cells carrying MotP/MotS and MotP/MotB stator can swim faster in liquid with high viscosity, MotP function is suggested to be important for the optimal function in elevated viscosity. In order to achieve optimal behavior in variable environments, these bacteria seem to evolve to use distinct sets of stator complexes or have additional components besides conventional stator proteins to fully exert motor rotation.

4. Molecular Physiology of Motor

4.1. Torque–speed relationship

To understand the mechanism of motor rotation, we need to know its basic properties: the power input and output, and their relationships. Measuring these properties of the motor involves technical difficulties, so

understanding of the motor physiology has been accompanied by technical development in the measurement system. Although the studies of power input for a single motor have still been hindered by such difficulties, one can measure the power output as the ''rotation'' by using a quite simple method that has been employed since the discovery of flagellar rotation. Cells are attached to a coverslip by a single flagellar filament and the rotation of each single motor is monitored by the resulting rotation of the cell body (Silverman and Simon, 1974). Such tethered cells rotate slowly (around 10 Hz) because of the large viscous load. Measurement of rotation of lightly loaded motors in swimming cells was achieved by a light scattering method under the microscope (Lowe et al., 1987), and values obtained by these two measurements were used for the initial estimation of a torque–speed relationship, an essential feature that characterizes the flagellar motor. The results showed a linear relationships: that as the speed increases, the torque linearly decreases.

To cover a wide range of the speed by the measurement of a single motor, the electrorotation method was developed (Berg and Turner, 1993; Iwazawa et al., 1993). In this technique, a tethered cell was spun under a rotating electric field that enabled motors to rotate up to several hundreds of Hertz. Measurement of the motor rotation has been carried out by this method, and revealed characteristic feature of the torque–speed relationships for the flagellar motor: for forward rotation, motor torque remained approximately constant up to speeds of about 60% of the zero-torque speed, then the torque dropped linearly with speed, crossed zero, and reached a minimum (Berg and Turner, 1993). In yet another approach, the cell body was fixed to the glass surface and a polystyrene bead was attached to a stub of one of its flagellar filaments (Ryu et al., 2000). By using beads of different sizes and changing the viscosity of external medium, one can measure motor torque under a wide range of speeds. The results confirmed the previous measurement by electrorotation method, showing the essentially constant torque and then linear decline as the speed increases (Chen and Berg, 2000b). The latter method allows us to measure the rotation at various conditions, such as different temperatures and using D_2O instead of H_2O for the effect of solvent isotope (Chen and Berg, 2000a). The results showed that in the low-speed regime, torque was independent of temperature, and solvent isotope effects were relatively small.

In the high–speed regime, torque was strongly dependent on temperature, as seen by a downward shift in the ''knee'' value, the region of the transition from constant torque to declining torque, at lower temperature. Also, solvent isotope effects were large. These results were consistent with previous studies for artificially energized cells of Streptococcus (Khan and Berg, 1983; Manson et al., 1980). Therefore, torque–speed relationship of the flagellar motor indicates that at low speeds, the motor operates near thermodynamic equilibrium, where rates of movement of the internal

mechanical components or translocation of protons are not rate-limiting, and that at high speeds, the rate-limiting step is proton transfer event, which results in the decline in torque at high speed. As discussed by Berry and Berg, a torque–speed relationship with this shape can be interpreted in the context of a simple three-state kinetic model and it suggests a rotation mechanism with a power stroke, in which motor rotation and dissipation of the energy available from proton transit occur synchronously (Berry and Berg, 1999). Fung and Berg (1995) found that when the motor operates in the low-speed regime near stall, its speed is proportional to the voltage applied across the inner cell membrane. Moreover, Gabel and Berg (2003) reported a linear relationship between speed (0–270 Hz) and PMF for light load on the motor. If we assume tightly coupled motor in which the translocation of a fixed number of protons drives each rotation, the linear speed–PMF relation is indicative of a simple voltage-gated proton channel.

Comparative studies have been reported for the Na^+-driven polar flagellar motor of *V. alginolyticus* (Sowa *et al.*, 2003). It has been shown that the torque–speed curve had the same shape as those of the wild-type *E. coli* motor and the hybrid motor with PomA/PotB chimeric stator in *E. coli* with full expression of the stator proteins: the torque is approximately constant (at $\sim$2200 pN nm) from stall up to a "knee" speed of $\sim$420 Hz, and then falls linearly with speed, extrapolating to zero torque at $\sim$910 Hz (Inoue *et al.*, 2008) (Fig. 2.9B). The overall shape of the torque–speed curve is quite similar to the H^+-driven *E. coli* motor described earlier, but the effect of the concentrations of the coupling ion on torque–speed curves of *V. alginolyticus* was different from those of *E. coli*. The curves for *E. coli* did not change even when the external environment had a pH value in the range of 4.7–8.8. However, when external NaCl concentrations were changed, the generated torque was changed over a wide range of speeds for *Vibrio* motor. This difference seems to be derived from not the mechanism of flagellar motors but the cell homeostasis when the concentration of the external coupling ion is varied. The Na^+-driven motor is likely to generate torque using basically the same mechanism as the H^+-driven motor.

4.2. Steps in rotation of motor

The rotation of the motor occurs by a sequence of discrete molecular events, presumably including the stages of ion binding in the stator followed by conformational changes in the stator that drive the rotor. Therefore, one can imagine that the motor behaves like a stepping motor. Since the discovery of flagellar rotation, such a step has been investigated but until recently it has not clearly demonstrated. The difficulty in observing rotational steps is due to the presence of an elastic linkage, the hook, between the tethered filament and the cell body, which smoothes the observed

rotation, and is also due to multiple independently functioning torque-generating units (stator complexes) per motor. One way to avoid this difficulty is to examine variations in rotation period. Such a stochastic analysis by assuming that intervals between steps follow a Poisson distribution led to an estimation of about 400 steps per revolution (Samuel and Berg, 1995). A similar analysis was done with motors containing only one or a few torque-generating units, and showed that the individual units step independently (Samuel and Berg, 1996).

Recently, direct observation of steps in the motor has been achieved by making a motor rotate as slow as possible in the work of Sowa et al (2005). The hybrid *E. coli* motor equipped with chimeric Na^+-driven stator complex PomA/PotB was used under the expression control of inducible promoter. Therefore, it was able to establish a motor with a small initial number of stator units, possibly one, by growing cells with low inducer level. Furthermore, by using the Na^+-type motor, the rotation rate can be reduced by lowering external Na^+ concentration. Motor rotation was detected by back-focal-plane (BFP) interferometry of 500-nm diameter beads attached to spontaneously sticky flagellar filament stub or by high-speed video recording of 200-nm diameter fluorescent beads attached in the same way. By using these experimental setups, the stepping rotations were observed at speeds below 7 and 40 Hz in BFP and fluorescence experiments, respectively. Interestingly, both backward and forward steps were observed at all speeds in both experiments, with higher probability at lower speeds. In this experiment, a *cheY* strain was used so that motor never rotates CW, thus backward steps represent microscopic reversibility rather than motor switching. Similar steps have been detected in the ATP-driven molecular motors. The step size was analyzed from these observations, and it was revealed that there is a peak at $13.7°$ (26 per revolution) and $-10.3°$ (35 per revolution) for forward and backward steps, respectively. Stepping motion in the ATP-driven molecular motors reflects both the discrete nature of the input energy and the periodicity of the "track" along which the motor runs (Mehta *et al.*, 1999; Schnitzer and Block, 1997; Yasuda *et al.*, 1998). Likewise, observation of 26 steps per revolution in the flagellar motor is consistent with the periodicity of the ring of FliG protein (see Section 2.3), suggesting that the motor steps along each FliG molecule in the rotor. Then how many ions can be translocated during one step? Because the simultaneous measurement of a single motor rotation and the ion translocation through the stator complex has not yet been established, we can only estimate it from the published parameters. It was reported that a wild-type *E. coli* cell with a PMF of about 150 mV drives a 1 μm bead with an estimated 280 pN nm per unit (Ryu *et al.*, 2000), suggesting that maximal step size for one ion in one unit would be $5°$ if all the input energy was consumed for the torque generation. Thus, there may be smaller substeps, or alternatively mechanical step may be coupled to

several ion translocations. As discussed in Section 2.4, the structural model for the stator complex proposed by the disulfide cross-linking study suggested two distinct channels per stator complex (Braun and Blair, 2001; Braun *et al.*, 2004), indicative of the latter possibility. In any case, the atomic model of the stator complex and establishment of simultaneous measurement system to investigate input–output relationships will be awaited for solving this problem.

4.3. Fluorescent imaging of motor

Recent development of single-molecule measurements of enzyme activities by using fluorescent microscopic methods makes it possible to reveal much about fundamental mechanisms of these protein machines. Toward the simultaneous measurement of the single motor rotation and ion flux through the stator complex, several attempts of fluorescent imaging of motor components have been undertaken. Our laboratory has used GFP for such an imaging *in vivo* (Fukuoka *et al.*, 2007, 2005). GFP was fused to the stator proteins, PomA and PomB of *V. alginolyticus*, and their behaviors *in vivo* were observed under the fluorescent microscope (Fukuoka *et al.*, 2005). By using this system, first, it was confirmed that GFP–PomA or GFP–PomB proteins were actually localized at the flagellated cell pole of *Vibrio*. Their polar localization requires the partner subunit (PomB or PomA) and the C-terminal domain of PomB that contains PGB motif required for anchoring the stator complexes to the motor. The polar localization of GFP-fused stator proteins was not observed in the absence of the polar flagellum. Finally, cells that express the PomA/GFP–PomB stator exhibited motility, although it was significantly reduced as compared with wild-type strain. Therefore, this is the initial success in imaging the functional stator proteins *in vivo*. Since the PomA/PomB stator complex assembles into the single polar flagellum of *Vibrio*, assembly of the stator complex at the flagellated cell pole can be observed as the polar localization of the GFP-fused stator proteins.

When we observed their behavior in the absence of Na^+, the coupling ion for polar flagellar motor of *Vibrio*, the GFP-fused stator proteins were not localized at the flagellated cell pole (Fukuoka *et al.*, submitted for publication). This effect appears to be Na^+–dependent and reversible, since addition of Na^+ in the medium restores the polar localization of the GFP-fused stators. The mutations of PomB D24, which is the binding site for Na^+, affected the localization. Therefore, stator assembly seems to be regulated by the energy source of the motor, the Na-motive force. This finding also suggested more dynamic behavior of the stator proteins than previously expected. These results are consistent with the previous reports

(Armitage and Evans, 1985; Evans and Armitage, 1985) and the recent report by Leake *et al*. (2006), demonstrating simultaneous measurement of the single motor rotation and the number and dynamics of GFP-fused MotB molecules in the motor in single molecule level by total internal reflection fluorescence (TIRF) microscopy. They tethered cells expressing GFP-MotB, and observed them under the TIRF or brightfield microscopy. TIRF images of tethered cells showed spots at the center of the cell rotation measured from brightfield images, indicating functional assembly of the stator consisting of GFP-MotB and MotA. Then they carried out stepwise photobleaching of single GFP-MotB in the motor. Counting fluorophores revealed that each motor contains around 22 copies of GFP-MotB, consistent with 11 stators reported by the recent resurrection experiment. They also reported by the analyses using FRAP and fluorescence loss in photobleaching methods that (1) there is a membrane pool of $\sim$200 GFP-MotB molecules diffusing at $\sim$0.008 μm^2 s^{-1}, and (2) turnover of GFP-MotB between the membrane pool and motor was observed with a rate constant of the order of 0.04 s^{-1}. Therefore, the static image of the ''stator'' is in need of change, and we need to understand its function under the consideration of more dynamic behavior. The stator complex appears to be transiently anchored around the rotor to generate torque, and rapidly exchanged when it worn or by responding to the change in energetic environment in the cell.

Fluorescent imaging of the rotor protein has also been attempted, and we were able to visualize functional GFP-FliG molecules in the center of the rotating tethered cell (Fukuoka *et al*., 2007). We are expecting that appropriate combination of functional GFP-fused stator and rotor protein in the motor may enable us to carry out measurement of FRET between stator and rotor components to demonstrate real-time imaging of rotor–stator interaction *in vivo*.

Imaging of the energy input into the motor is another big challenge. Recently, using a fluorescent probe for Na$^+$, Sodium Green, intracellular Na$^+$ concentration in single *E. coli* cells has been measured (Lo *et al*., 2006). This method requires low-light electron-multiplying charge-coupled device camera and laser fluorescence microscopy, and makes it possible to measure intracellular Na$^+$ of a series of 50 single cells, without any detectable effect on the flagellar motor. The values obtained are consistent with the ones measured by other methods. Likewise, fluorescence technique to measure membrane potential in single cell has been established by using the dye tetramethylrhodamine methyl ester (Lo *et al*., 2007). These fluorescence techniques to measure input energy (membrane potential and ion gradient) together with the rotation analysis in the single molecule level finally open the new era for motor physiology that would make it possible to visualize input–output relationships in real time and *in vivo*.

5. Conclusion

In addition to the proton-driven motor, the Na^+-driven motor has been studied extensively and many important data have accumulated. Using these insights, a genetic manipulation of the Na^+-driven *E. coli* hybrid motor with chimeric stator led us to a recent breakthrough to observe directly the steps in rotation of a single motor, the basic process of the motor. From now on, we can expect to elucidate the rotation mechanism by discussing the input and output relations of the energy during a single step in a rotation. Moreover, the technology of single-molecule fluorescent observation has been introduced, and it will be able to visualize a dynamic interaction between rotor and stator. To understand the mechanism of energy conversion that changes the ion flux into the mechanical power, the crystal structures of the membrane motor proteins are also needed. We would like to learn the biological nature from the tiny nanomachine of the bacterial flagella.

REFERENCES

Aizawa, S., Dean, G. E., Jones, C. J., Macnab, R. M., and Yamaguchi, S. (1985). Purification and characterization of the flagellar hook-basal body complex of *Salmonella typhimurium*. *J. Bacteriol.* **161,** 836–849.

Akiba, T., Yoshimura, H., and Namba, K. (1991). Monolayer crystallization of flagellar L-P rings by sequential addition and depletion of lipid. *Science* **252,** 1544–1546.

Aldridge, P., Karlinsey, J. E., Becker, E., Chevance, F. F., and Hughes, K. T. (2006). Flk prevents premature secretion of the anti-sigma factor FlgM into the periplasm. *Mol. Microbiol.* **60,** 630–643.

Armitage, J. P. (1999). Bacterial tactic responses. *Adv. Microb. Physiol.* **41,** 229–289.

Armitage, J. P., and Evans, M. C. W. (1985). Control of the proton-motive force in *Rhodopseudomonas sphaeroides* in the light and dark and its effect on the initiation of flagellar rotation. *Biochimica Biophysica Acta* **806,** 42–45.

Armitage, J. P., and Macnab, R. M. (1987). Unidirectional, intermittent rotation of the flagellum of *Rhodobacter sphaeroides*. *J. Bacteriol.* **169,** 514–518.

Asai, Y., Kojima, S., Kato, H., Nishioka, N., Kawagishi, I., and Homma, M. (1997). Putative channel components for the fast-rotating sodium-driven flagellar motor of a marine bacterium. *J. Bacteriol.* **179,** 5104–5110.

Asai, Y., Kawagishi, I., Sockett, R. E., and Homma, M. (1999). Hybrid motor with H^+- and Na^+-driven components can rotate *Vibrio* polar flagella by using sodium ions. *J. Bacteriol.* **181,** 6332–6338.

Asai, Y., Kawagishi, I., Sockett, R. E., and Homma, M. (2000). Coupling ion specificity of chimeras between H^+- and Na^+-driven motor proteins, MotB and PomB, in *Vibrio* polar flagella. *EMBO J.* **19,** 3639–3648.

Asai, Y., Yakushi, T., Kawagishi, I., and Homma, M. (2003). Ion-coupling determinants of Na^+-driven and H^+-driven flagellar motors. *J. Mol. Biol.* **327,** 453–463.

Asakura, S. (1970). Polymerization of flagellin and polymorphism of flagella. *Adv. Biophys.* **1,** 99–155.

Atsumi, T., Sugiyama, S., Cragoe, E. J., Jr., and Imae, Y. (1990). Specific inhibition of the Na$^+$-driven flagellar motors of alkalophilic *Bacillus* strains by the amiloride analog phenamil. *J. Bacteriol.* **172,** 1634–1639.

Atsumi, T., McCarter, L., and Imae, Y. (1992). Polar and lateral flagellar motors of marine *Vibrio* are driven by different ion-motive forces. *Nature* **355,** 182–184.

Attmannspacher, U., Scharf, B., and Schmitt, R. (2005). Control of speed modulation (chemokinesis) in the unidirectional rotary motor of *Sinorhizobium meliloti*. *Mol. Microbiol.* **56,** 708–718.

Bange, G., Petzold, G., Wild, K., Parlitz, R. O., and Sinning, I. (2007). The crystal structure of the third signal-recognition particle GTPase FlhF reveals a homodimer with bound GTP. *Proc. Natl. Acad. Sci. USA* **104,** 13621–13625.

Bennett, J. C., Thomas, J., Fraser, G. M., and Hughes, C. (2001). Substrate complexes and domain organization of the *Salmonella* flagellar export chaperones FlgN and FliT. *Mol. Microbiol.* **39,** 781–791.

Berg, H. C. (2003). The rotary motor of bacterial flagella. *Annu. Rev. Biochem.* **72,** 19–54.

Berg, H. C., and Anderson, R. A. (1973). Bacteria swim by rotating their flagellar filaments. *Nature* **245,** 380–382.

Berg, H. C., and Turner, L. (1993). Torque generated by the flagellar motor of *Escherichia coli*. *Biophys. J.* **65,** 2201–2216.

Berry, R. M., and Armitage, J. P. (1999). The bacterial flagella motor. *Adv. Microb. Physiol.* **41,** 291–337.

Berry, R. M., and Berg, H. C. (1999). Torque generated by the flagellar motor of *Escherichia coli* while driven backward. *Biophys. J.* **76,** 580–587.

Blair, D. F., and Berg, H. C. (1988). Restoration of torque in defective flagellar motors. *Science* **242,** 1678–1681.

Blair, D. F., and Berg, H. C. (1990). The MotA protein of *E. coli* is a proton-conducting component of the flagellar motor. *Cell* **60,** 439–449.

Block, S. M., and Berg, H. C. (1984). Successive incorporation of force-generating units in the bacterial rotary motor. *Nature* **309,** 470–472.

Braun, T. F., and Blair, D. F. (2001). Targeted disulfide cross-linking of the MotB protein of *Escherichia coli*: Evidence for two H$^+$ channels in the stator complex. *Biochemistry* **40,** 13051–13059.

Braun, T. F., Poulson, S., Gully, J. B., Empey, J. C., Van Way, S., Putnam, A., and Blair, D. F. (1999). Function of proline residues of MotA in torque generation by the flagellar motor of *Escherichia coli*. *J. Bacteriol.* **181,** 3542–3551.

Braun, T. F., Al-Mawsawi, L. Q., Kojima, S., and Blair, D. F. (2004). Arrangement of core membrane segments in the MotA/MotB proton-channel complex of *Escherichia coli*. *Biochemistry* **43,** 35–45.

Brown, P. N., Hill, C. P., and Blair, D. F. (2002). Crystal structure of the middle and C-terminal domains of the flagellar rotor protein FliG. *EMBO J.* **21,** 3225–3234.

Brown, P. N., Mathews, M. A., Joss, L. A., Hill, C. P., and Blair, D. F. (2005). Crystal structure of the flagellar rotor protein FliN from *Thermotoga maritima*. *J. Bacteriol.* **187,** 2890–2902.

Brown, P. N., Terrazas, M., Paul, K., and Blair, D. F. (2007). Mutational analysis of the flagellar protein FliG: Sites of interaction with FliM and implications for organization of the switch complex. *J. Bacteriol.* **189,** 305–312.

Calladine, C. R. (1978). Change of wave form in bacterial flagella: The role of mechanics at the molecular level. *J. Mol. Biol.* **118,** 457–479.

Chen, X., and Berg, H. C. (2000a). Solvent-isotope and pH effects on flagellar rotation in *Escherichia coli*. *Biophys. J.* **78,** 2280–2284.

Chen, X., and Berg, H. C. (2000b). Torque-speed relationship of the flagellar rotary motor of *Escherichia coli*. *Biophys. J.* **78,** 1036–1041.

Chevance, F. F., Takahashi, N., Karlinsey, J. E., Gnerer, J., Hirano, T., Samudrala, R., Aizawa, S., and Hughes, K. T. (2007). The mechanism of outer membrane penetration by the eubacterial flagellum and implications for spirochete evolution. *Genes Dev.* **21,** 2326–2335.

Chilcott, G. S., and Hughes, K. T. (2000). Coupling of flagellar gene expression to flagellar assembly in *Salmonella enterica* serovar *typhimurium* and *Escherichia coli*. *Microbiol. Mol. Biol. Rev.* **64,** 694–708.

Chun, S. Y., and Parkinson, J. S. (1988). Bacterial motility: Membrane topology of the *Escherichia coli* MotB protein. *Science* **239,** 276–278.

Claret, L., Calder, S. R., Higgins, M., and Hughes, C. (2003). Oligomerization and activation of the FliI ATPase central to bacterial flagellum assembly. *Mol. Microbiol.* **48,** 1349–1355.

Cluzel, P., Surette, M., and Leibler, S. (2000). An ultrasensitive bacterial motor revealed by monitoring signaling proteins in single cells. *Science* **287,** 1652–1655.

Cordell, S. C., and Lowe, J. (2001). Crystal structure of the bacterial cell division regulator MinD. *FEBS Lett.* **492,** 160–165.

Cornelis, G. R. (2006). The type III secretion injectisome. *Nat. Rev. Microbiol.* **4,** 811–825.

Dailey, F. E., and Berg, H. C. (1993). Mutants in disulfide bond formation that disrupt flagellar assembly in *Escherichia coli*. *Proc. Natl. Acad. Sci. USA* **90,** 1043–1047.

De Mot, R., and Vanderleyden, J. (1994). The C-terminal sequence conservation between OmpA-related outer membrane proteins and MotB suggests a common function in both Gram-positive and Gram-negative bacteria, possibly in the interaction of these domains with peptidoglycan. *Mol. Microbiol.* **12,** 333–334.

Dean, G. D., Macnab, R. M., Stader, J., Matsumura, P., and Burks, C. (1984). Gene sequence and predicted amino acid sequence of the motA protein, a membrane-associated protein required for flagellar rotation in *Escherichia coli*. *J. Bacteriol.* **159,** 991–999.

Doyle, T. B., Hawkins, A. C., and McCarter, L. L. (2004). The complex flagellar torque generator of *Pseudomonas aeruginosa*. *J. Bacteriol.* **186,** 6341–6350.

Dyer, C. M., and Dahlquist, F. W. (2006). Switched or not? The structure of unphosphorylated CheY bound to the N-terminus of FliM. *J. Bacteriol.* **188,** 7354–7363.

Eggenhofer, E., Haslbeck, M., and Scharf, B. (2004). MotE serves as a new chaperone specific for the periplasmic motility protein, MotC, in *Sinorhizobium meliloti*. *Mol. Microbiol.* **52,** 701–712.

Evans, M. C. W., and Armitage, J. P. (1985). Initiation of flagellar rotation in *Rhodopsudomonas sphaeroides*. *FEBS Lett.* **186,** 93–97.

Fahrner, K. A., Block, S. M., Krishnaswamy, S., Parkinson, J. S., and Berg, H. C. (1994). A mutant hook-associated protein (HAP3) facilitates torsionally induced transformations of the flagellar filament of *Escherichia coli*. *J. Mol. Biol.* **238,** 173–186.

Fan, F., and Macnab, R. M. (1996). Enzymatic characterization of FliI—An ATPase involved in flagellar assembly in *Salmonella typhimurium*. *J. Biol. Chem.* **271,** 31981–31988.

Fan, F., Ohnishi, K., Francis, N. R., and Macnab, R. M. (1997). The FliP and FliR proteins of *Salmonella typhimurium*, putative components of the type III flagellar export apparatus, are located in the flagellar basal body. *Mol. Microbiol.* **26,** 1035–1046.

Ferris, H. U., and Minamino, T. (2006). Flipping the switch: Bringing order to flagellar assembly. *Trends Microbiol.* **14,** 519–526.

Focia, P. J., Shepotinovskaya, I. V., Seidler, J. A., and Freymann, D. M. (2004). Heterodimeric GTPase core of the SRP targeting complex. *Science* **303,** 373–377.

Francis, N. R., Irikura, V. M., Yamaguchi, S., DeRosier, D. J., and Macnab, R. M. (1992). Localization of the *Salmonella typhimurium* flagellar switch protein FliG to the cytoplasmic M-ring face of the basal body. *Proc. Natl. Acad. Sci. USA* **89,** 6304–6308.

Francis, N. R., Sosinsky, G. E., Thomas, D., and DeRosier, D. J. (1994). Isolation, characterization and structure of bacterial flagellar motors containing the switch complex. *J. Mol. Biol.* **235,** 1261–1270.

Fraser, G. M., Bennett, J. C., and Hughes, C. (1999). Substrate-specific binding of hook-associated proteins by FlgN and FliT, putative chaperones for flagellum assembly. *Mol. Microbiol.* **32,** 569–580.

Fraser, G. M., Gonzalez-Pedrajo, B., Tame, J. R., and Macnab, R. M. (2003). Interactions of FliJ with the *Salmonella* type III flagellar export apparatus. *J. Bacteriol.* **185,** 5546–5554.

Fukuoka, H., Yakushi, T., Kusumoto, A., and Homma, M. (2005). Assembly of motor proteins, PomA and PomB, in the Na^+-driven stator of the flagellar motor. *J. Mol. Biol.* **351,** 707–717.

Fukuoka, H., Sowa, Y., Kojima, S., Ishijima, A., and Homma, M. (2007). Visualization of functional rotor proteins of the bacterial flagellar motor in the cell membrane. *J. Mol. Biol.* **367,** 692–701.

Fung, D. C., and Berg, H. C. (1995). Powering the flagellar motor of *Escherichia coli* with an external voltage source. *Nature* **375,** 809–812.

Gabel, C. V., and Berg, H. C. (2003). The speed of the flagellar rotary motor of *Escherichia coli* varies linearly with protonmotive force. *Proc. Natl. Acad. Sci. USA* **100,** 8748–8751.

Gillen, K., and Hughes, K. T. (1991). Negative regulatory loci coupling flagellin synthesis to flagellar assembly in *Salmonella typhimurium. J. Bacteriol.* **173,** 2301–2310.

Gonzalez-Pedrajo, B., Minamino, T., Kihara, M., and Namba, K. (2006). Interactions between C ring proteins and export apparatus components: A possible mechanism for facilitating type III protein export. *Mol. Microbiol.* **60,** 984–998.

Gotz, R., and Schmitt, R. (1987). *Rhizobium meliloti* swims by unidirectional, intermittent rotation of right-handed flagellar helices. *J. Bacteriol.* **169,** 3146–3150.

Hirano, T., Yamaguchi, S., Oosawa, K., and Aizawa, S. I. (1994). Roles of FliK and FlhB in determination of flagellar hook length in *Salmonella typhimurium. J. Bacteriol.* **176,** 5439–5449.

Hizukuri, Y., Yakushi, T., Kawagishi, I., and Homma, M. (2006). Role of the intramolecular disulfide bond in FlgI, the flagellar P-ring component of *Escherichia coli. J. Bacteriol.* **188,** 4190–4197.

Homma, M., and Iino, T. (1985). Locations of hook-associated proteins in flagellar structures of *Salmonella typhimurium. J. Bacteriol.* **162,** 183–189.

Homma, M., Fujita, H., Yamaguchi, S., and Iino, T. (1984). Excretion of unassembled flagellin by *Salmonella typhimurium* mutants deficient in the hook-associated proteins. *J. Bacteriol.* **159,** 1056–1059.

Homma, M., Iino, T., Kutsukake, K., and Yamaguchi, S. (1986). *In vitro* reconstitution of flagellar filaments onto hooks of filamentless mutants of *Salmonella typhimurium* by addition of hook-associated proteins. *Proc. Natl. Acad. Sci. USA* **83,** 6169–6173.

Homma, M., Komeda, Y., Iino, T., and Macnab, R. M. (1987). The *flaFIX* gene product of *Salmonella typhimurium* is a flagellar basal body component with a signal peptide for export. *J. Bacteriol.* **169,** 1493–1498.

Homma, M., Kutsukake, K., Hasebe, M., Iino, T., and Macnab, R. M. (1990). FlgB, FlgC, FlgF and FlgG. A family of structurally related proteins in the flagellar basal body of *Salmonella typhimurium. J. Mol. Biol.* **211,** 465–477.

Hosking, E. R., Vogt, C., Bakker, E. P., and Manson, M. D. (2006). The *Escherichia coli* MotAB proton channel unplugged. *J. Mol. Biol.* **364,** 921–937.

Hueck, C. J. (1998). Type III protein secretion systems in bacterial pathogens of animals and plants. *Microbiol. Mol. Biol. Rev.* **62,** 379–433.

Hughes, K. T., Gillen, K. L., Semon, M. J., and Karlinsey, J. E. (1993). Sensing structural intermediates in bacterial flagellar assembly by export of a negative regulator. *Science* **262,** 1277–1280.

Hunte, C., Screpanti, E., Venturi, M., Rimon, A., Padan, E., and Michel, H. (2005). Structure of a Na$^+$/H$^+$ antiporter and insights into mechanism of action and regulation by pH. *Nature* **435,** 1197–1202.

Iino, T. (1969). Genetics and chemistry of bacterial flagella. *Bacteriol. Rev.* **33,** 454–475.

Ikeda, T., Asakura, S., and Kamiya, R. (1985). ''Cap'' on the tip of *Salmonella* flagella. *J. Mol. Biol.* **184,** 735–737.

Ikeda, T., Homma, M., Iino, T., Asakura, S., and Kamiya, R. (1987). Localization and stoichiometry of hook-associated proteins within *Salmonella typhimurium* flagella. *J. Bacteriol.* **169,** 1168–1173.

Ikeda, T., Yamaguchi, S., and Hotani, H. (1993). Flagellar growth in a filament-less *Salmonella* fliD mutant supplemented with purified hook-associated protein-2. *J. Biochem. (Tokyo)* **114,** 39–44.

Imada, K., Minamino, T., Tahara, A., and Namba, K. (2007). Structural similarity between the flagellar type III ATPase FliI and F$_1$-ATPase subunits. *Proc. Natl. Acad. Sci. USA* **104,** 485–490.

Imae, Y., and Atsumi, T. (1989). Na$^+$-driven bacterial flagellar motors. *J. Bioenerg. Biomembr.* **21,** 705–716.

Inoue, Y., Lo, C. J., Fukuoka, H., Takahashi, H., Sowa, Y., Pilizota, T., Wadhams, G. H., Homma, M., Berry, R. M., and Ishijima, A. (2008). Torque-speed relationships of Na$^+$-driven chimeric flagellar motors in *Escherichia coli*. *J. Mol. Biol.* **376,** 1251–1259.

Ito, M., Hicks, D. B., Henkin, T. M., Guffanti, A. A., Powers, B. D., Zvi, L., Uematsu, K., and Krulwich, T. A. (2004). MotPS is the stator-force generator for motility of alkaliphilic *Bacillus*, and its homologue is a second functional Mot in *Bacillus subtilis*. *Mol. Microbiol.* **53,** 1035–1049.

Ito, M., Terahara, N., Fujinami, S., and Krulwich, T. A. (2005). Properties of motility in *Bacillus subtilis* powered by the H$^+$-coupled MotAB flagellar stator, Na$^+$-coupled MotPS or hybrid stators MotAS or MotPB. *J. Mol. Biol.* **352,** 396–408.

Iwazawa, J., Imae, Y., and Kobayasi, S. (1993). Study of the torque of the bacterial flagellar motor using a rotating electric field. *Biophys. J.* **64,** 925–933.

Jaques, S., Kim, Y. K., and McCarter, L. L. (1999). Mutations conferring resistance to phenamil and amiloride, inhibitors of sodium-driven motility of *Vibrio parahaemolyticus*. *Proc. Natl. Acad. Sci. USA* **96,** 5740–5745.

Kamiya, R., and Asakura, S. (1976). Helical transformations of *Salmonella* flagella *in vitro*. *J. Mol. Biol.* **106,** 167–186.

Karlinsey, J. E., Pease, A. J., Winkler, M. E., Bailey, J. L., and Hughes, K. T. (1997). The *flk* gene of *Salmonella typhimurium* couples flagellar P- and L-ring assembly to flagellar morphogenesis. *J. Bacteriol.* **179,** 2389–2400.

Katayama, E., Shiraishi, T., Oosawa, K., Baba, N., and Aizawa, S. (1996). Geometry of the flagellar motor in the cytoplasmic membrane of *Salmonella typhimurium* as determined by stereo-photogrammetry of quick-freeze deep-etch replica images. *J. Mol. Biol.* **255,** 458–475.

Khan, S., and Berg, H. C. (1983). Isotope and thermal effects in chemiosmotic coupling to the flagellar motor of *Streptococcus*. *Cell* **32,** 913–919.

Khan, S., Dapice, M., and Reese, T. S. (1988). Effects of *mot* gene expression on the structure of the flagellar motor. *J. Mol. Biol.* **202,** 575–584.

Kobayashi, K., Saitoh, T., Shah, D. S., Ohnishi, K., Goodfellow, I. G., Sockett, R. E., and Aizawa, S. I. (2003). Purification and characterization of the flagellar basal body of *Rhodobacter sphaeroides*. *J. Bacteriol.* **185,** 5295–5300.

Koebnik, R. (1995). Proposal for a peptidoglycan-associating alpha-helical motif in the C-terminal regions of some bacterial cell-surface proteins. *Mol. Microbiol.* **16,** 1269–1270.

Kojima, S., and Blair, D. F. (2001). Conformational change in the stator of the bacterial flagellar motor. *Biochemistry* **40,** 13041–13050.

Kojima, S., and Blair, D. F. (2004a). The bacterial flagellar motor: Structure and function of a complex molecular machine. *Int. Rev. Cytol.* **233,** 93–134.

Kojima, S., and Blair, D. F. (2004b). Solubilization and purification of the MotA/MotB complex of *Escherichia coli. Biochemistry* **43,** 26–34.

Kojima, S., Atsumi, T., Muramoto, K., Kudo, S., Kawagishi, I., and Homma, M. (1997). *Vibrio alginolyticus* mutants resistant to phenamil, a specific inhibitor of the sodium–driven flagellar motor. *J. Mol. Biol.* **265,** 310–318.

Kojima, S., Asai, Y., Atsumi, T., Kawagishi, I., and Homma, M. (1999). Na^+–driven flagellar motor resistant to phenamil, an amiloride analog, caused by mutations in putative channel components. *J. Mol. Biol.* **285,** 1537–1547.

Kojima, S., Shoji, T., Asai, Y., Kawagishi, I., and Homma, M. (2000). A slow–motility phenotype caused by substitutions at residue Asp31 in the PomA channel component of a sodium–driven flagellar motor. *J. Bacteriol.* **182,** 3314–3318.

Kojima, M., Kubo, R., Yakushi, T., Homma, M., and Kawagishi, I. (2007). The bidirectional polar and unidirectional lateral flagellar motors of *Vibrio alginolyticus* are controlled by a single CheY species. *Mol. Microbiol.* **64,** 57–67.

Kojima, S., Shinohara, A., Terashima, H., Yakushi, T., Sakuma, M., Homma, M., Namba, K., and Imada, K. (2008). Insights into the stator assembly of the *Vibrio* flagellar motor from the crystal structure of MotY. *Proc. Natl. Acad. Sci. USA* **190,** 7696–7701.

Kubori, T., Shimamoto, N., Yamaguchi, S., Namba, K., and Aizawa, S. (1992). Morphological pathway of flagellar assembly in *Salmonella typhimurium. J. Mol. Biol.* **226,** 433–446.

Kudo, S., Magariyama, Y., and Aizawa, S.-I. (1990). Abrupt changes in flagellar rotation observed by laser dark–field microscopy. *Nature* **346,** 677–680.

Kusumoto, A., Kamisaka, K., Yakushi, T., Terashima, H., Shinohara, A., and Homma, M. (2006). Regulation of polar flagellar number by the *flhF* and *flhG* genes in *Vibrio alginolyticus. J. Biochem. (Tokyo)* **139,** 113–121.

Kusumoto, A., Shinohara, A., Terashima, H., Kojima, S., Yakushi, T., and Homma, M. (2008). Collaboration of FlhF and FlhG to regulate polar-flagella number and localization in *Vibrio alginolyticus. Microbiology* **154,** 1390–1399.

Kutsukake, K. (1994). Excretion of the anti–sigma factor through a flagellar substructure couples flagellar gene expression with flagellar assembly in *Salmonella typhimurium. Mol. Gen. Genet.* **243,** 605–612.

Kutsukake, K. (1997). Hook–length control of the export–switching machinery involves a double–locked gate in *Salmonella typhimurium* flagellar morphogenesis. *J. Bacteriol.* **179,** 1268–1273.

Kutsukake, K., and Iino, T. (1994). Role of the FliA–FlgM regulatory system on the transcriptional control of the flagellar regulon and flagellar formation in *Salmonella typhimurium. J. Bacteriol.* **176,** 3598–3605.

Kutsukake, K., Ohya, Y., and Iino, T. (1990). Transcriptional analysis of the flagellar regulon of *Salmonella typhimurium. J. Bacteriol.* **172,** 741–747.

Kutsukake, K., Minamino, T., and Yokoseki, T. (1994). Isolation and characterization of FliK-independent flagellation mutants from *Salmonella typhimurium. J. Bacteriol.* **176,** 7625–7629.

Leake, M. C., Chandler, J. H., Wadhams, G. H., Bai, F., Berry, R. M., and Armitage, J. P. (2006). Stoichiometry and turnover in single, functioning membrane protein complexes. *Nature* **443,** 355–358.

Lee, S. Y., Cho, H. S., Pelton, J. G., Yan, D., Henderson, R. K., King, D. S., Huang, L., Kustu, S., Berry, E. A., and Wemmer, D. E. (2001). Crystal structure of an activated response regulator bound to its target. *Nat. Struct. Biol.* **8,** 52–56.

Liu, X., and Matsumura, P. (1994). The FlhD/FlhC complex, a transcriptional activator of the *Escherichia coli* flagellar class II operons. *J. Bacteriol.* **176,** 7345–7351.

Lloyd, S. A., and Blair, D. F. (1997). Charged residues of the rotor protein FliG essential for torque generation in the flagellar motor of *Escherichia coli*. *J. Mol. Biol.* **266,** 733–744.

Lloyd, S. A., Tang, H., Wang, X., Billings, S., and Blair, D. F. (1996). Torque generation in the flagellar motor of *Escherichia coli*: Evidence of a direct role for FliG but not for FliM or FliN. *J. Bacteriol.* **178,** 223–231.

Lloyd, S. A., Whitby, F. G., Blair, D. F., and Hill, C. P. (1999). Structure of the C-terminal domain of FliG, a component of the rotor in the bacterial flagellar motor. *Nature* **400,** 472–475.

Lo, C. J., Leake, M. C., and Berry, R. M. (2006). Fluorescence measurement of intracellular sodium concentration in single *Escherichia coli* cells. *Biophys. J.* **90,** 357–365.

Lo, C. J., Leake, M. C., Pilizota, T., and Berry, R. M. (2007). Nonequivalence of membrane voltage and ion-gradient as driving forces for the bacterial flagellar motor at low load. *Biophys. J.* **93,** 294–302.

Lowe, G., Meister, M., and Berg, H. C. (1987). Rapid rotation of flagellar bundles in swimming bacteria. *Nature* **325,** 637–640.

Luirink, J., and Sinning, I. (2004). SRP-mediated protein targeting: Structure and function revisited. *Biochim. Biophys. Acta* **1694,** 17–35.

Macnab, R. M. (2003). How bacteria assemble flagella. *Annu. Rev. Microbiol.* **57,** 77–100.

Macnab, R. M. (2004). Type III flagellar protein export and flagellar assembly. *Biochim. Biophys. Acta* **1694,** 207–217.

Macnab, R. M., and Ornston, M. K. (1977). Normal-to-curly flagellar transitions and their role in bacterial tumbling. Stabilization of an alternative quaternary structure by mechanical force. *J. Mol. Biol.* **112,** 1–30.

Manson, M. D., Tedesco, P. M., and Berg, H. C. (1980). Energetics of flagellar rotation in bacteria. *J. Mol. Biol.* **138,** 541–561.

Marykwas, D. L., Schmidt, S. A., and Berg, H. C. (1996). Interacting components of the flagellar motor of *Escherichia coli* revealed by the two-hybrid system in yeast. *J. Mol. Biol.* **256,** 564–576.

Mathews, M. A., Tang, H. L., and Blair, D. F. (1998). Domain analysis of the FliM protein of *Escherichia coli*. *J. Bacteriol.* **180,** 5580–5590.

McCarter, L. L. (1994a). MotX, the channel component of the sodium-type flagellar motor. *J. Bacteriol.* **176,** 5988–5998.

McCarter, L. L. (1994b). MotY, a component of the sodium-type flagellar motor. *J. Bacteriol.* **176,** 4219–4225.

McCarter, L. L. (2001). Polar flagellar motility of the Vibrionaceae. *Microbiol. Mol. Biol. Rev.* **65,** 445–462.

McCarter, L. L. (2004). Dual flagellar systems enable motility under different circumstances. *J. Mol. Microbiol. Biotechnol.* **7,** 18–29.

McCarter, L., Hilmen, M., and Silverman, M. (1988). Flagellar dynamometer controls warmer cell differentiation of *V. parahaemolyticus*. *Cell* **54,** 345–351.

McMurry, J. L., Murphy, J. W., and Gonzalez-Pedrajo, B. (2006). The FliN-FliH interaction mediates localization of flagellar export ATPase FliI to the C ring complex. *Biochemistry* **45,** 11790–11798.

Mehta, A. D., Rock, R. S., Rief, M., Spudich, J. A., Mooseker, M. S., and Cheney, R. E. (1999). Myosin-V is a processive actin-based motor. *Nature* **400,** 590–593.

Mimori, Y., Yamashita, I., Murata, K., Fujiyoshi, Y., Yonekura, K., Toyoshima, C., and Namba, K. (1995). The structure of the R-type straight flagellar filament of *Salmonella* at 9 angstrom resolution by electron cryomicroscopy. *J. Mol. Biol.* **249,** 69–87.

Minamino, T., and Macnab, R. M. (1999). Components of the *Salmonella* flagellar export apparatus and classification of export substrates. *J. Bacteriol.* **181,** 1388–1394.

Minamino, T., and Macnab, R. M. (2000a). FliH, a soluble component of the type III flagellar export apparatus of Salmonella, forms a complex with FliI and inhibits its ATPase activity. *Mol. Microbiol.* **37,** 1494–1503.

Minamino, T., and Macnab, R. M. (2000b). Interactions among components of the *Salmonella* flagellar export apparatus and its substrates. *Mol. Microbiol.* **35,** 1052–1064.

Minamino, T., and Namba, K. (2004). Self-assembly and type III protein export of the bacterial flagellum. *J. Mol. Microbiol. Biotechnol.* **7,** 5–17.

Minamino, T., Doi, H., and Kutsukake, K. (1999). Substrate specificity switching of the flagellum-specific export apparatus during flagellar morphogenesis in *Salmonella typhimurium*. *Biosci. Biotechnol. Biochem.* **63,** 1301–1303.

Minamino, T., Chu, R., Yamaguchi, S., and Macnab, R. M. (2000a). Role of FliJ in flagellar protein export in *Salmonella*. *J. Bacteriol.* **182,** 4207–4215.

Minamino, T., Yamaguchi, S., and Macnab, R. M. (2000b). Interaction between FliE and FlgB, a proximal rod component of the flagellar basal body of *Salmonella*. *J. Bacteriol.* **182,** 3029–3036.

Minamino, T., Kazetani, K., Tahara, A., Suzuki, H., Furukawa, Y., Kihara, M., and Namba, K. (2006). Oligomerization of the bacterial flagellar ATPase FliI is controlled by its extreme N-terminal region. *J. Mol. Biol.* **360,** 510–519.

Morgan, D. G., Owen, C., Melanson, L. A., and Derosier, D. J. (1995). Structure of bacterial flagellar filaments at 11 angstrom resolution: Packing of the alpha-helices. *J. Mol. Biol.* **249,** 88–110.

Moriya, N., Minamino, T., Hughes, K. T., Macnab, R. M., and Namba, K. (2006). The type III flagellar export specificity switch is dependent on FliK ruler and a molecular clock. *J. Mol. Biol.* **359,** 466–477.

Murata, T., Yamato, I., Kakinuma, Y., Leslie, A. G., and Walker, J. E. (2005). Structure of the rotor of the V-Type Na^+-ATPase from *Enterococcus hirae*. *Science* **308,** 654–659.

Murphy, G. E., Leadbetter, J. R., and Jensen, G. J. (2006). *In situ* structure of the complete *Treponema primitia* flagellar motor. *Nature* **442,** 1062–1064.

Nambu, T., and Kutsukake, K. (2000). The *Salmonella* FlgA protein, a putativeve periplasmic chaperone essential for flagellar P ring formation. *Microbiology* **146,** 1171–1178.

Nambu, T., Minamino, T., Macnab, R. M., and Kutsukake, K. (1999). Peptidoglycan-hydrolyzing activity of the FlgJ protein, essential for flagellar rod formation in *Salmonella typhimurium*. *J. Bacteriol.* **181,** 1555–1561.

Obara, M., Yakushi, T., Kojima, S., and Homma, M. (2008). Roles of charged residues in the C-terminal region of PomA, a stator component of the Na^+-driven flagellar motor. *J. Bacteriol.* **190,** 3565–3571.

Ohnishi, K., Kusukake, K., Suzuki, H., and Iino, T. (1990). Gene FliA encodes an alternative sigma factor specific for flagellar operons in *Salmonella typhimurium*. *Mol. Gen. Genet.* **221,** 139–147.

Ohnishi, K., Kutsukake, K., Suzuki, H., and Iino, T. (1992). A novel transcriptional regulation mechanism in the flagellar regulon of *Salmonella typhimurium*—An anti-sigma factor inhibits the activity of the flagellum-specific sigma factor, sigmaF. *Mol. Microbiol.* **6,** 3149–3157.

Okabe, M., Yakushi, T., Asai, Y., and Homma, M. (2001). Cloning and characterization of *motX*, a *Vibrio alginolyticus* sodium-driven flagellar motor gene. *J. Biochem. (Tokyo)* **130,** 879–884.

Okabe, M., Yakushi, T., and Homma, M. (2005). Interactions of MotX with MotY and with the PomA/PomB sodium ion channel complex of the *Vibrio alginolyticus* polar flagellum. *J. Biol. Chem.* **280,** 25659–25664.

Okunishi, I., Kawagishi, I., and Homma, M. (1996). Cloning and characterization of *motY*, a gene coding for a component of the sodium-driven flagellar motor in *Vibrio alginolyticus*. *J. Bacteriol.* **178,** 2409–2415.

Oosawa, K., Ueno, T., and Aizawa, S. (1994). Overproduction of the bacterial flagellar switch proteins and their interactions with the MS ring complex *in vitro*. *J. Bacteriol*. **176,** 3683–3691.

Pandza, S., Baetens, M., Park, C. H., Au, T., Keyhan, M., and Matin, A. (2000). The G-protein FlhF has a role in polar flagellar placement and general stress response induction in *Pseudomonas putida*. *Mol. Microbiol*. **36,** 414–423.

Park, S. Y., Lowder, B., Bilwes, A. M., Blair, D. F., and Crane, B. R. (2006). Structure of FliM provides insight into assembly of the switch complex in the bacterial flagella motor. *Proc. Natl. Acad. Sci. USA* **103,** 11886–11891.

Parkinson, J. S. (2003). Bacterial chemotaxis: A new player in response regulator dephosphorylation. *J. Bacteriol*. **185,** 1492–1494.

Parkinson, J. S., Ames, P., and Studdert, C. A. (2005). Collaborative signaling by bacterial chemoreceptors. *Curr. Opin. Microbiol*. **8,** 116–121.

Paul, K., and Blair, D. F. (2006). Organization of FliN subunits in the flagellar motor of *Escherichia coli*. *J. Bacteriol*. **188,** 2502–2511.

Paul, K., Harmon, J. G., and Blair, D. F. (2006). Mutational analysis of the flagellar rotor protein FliN: Identification of surfaces important for flagellar assembly and switching. *J. Bacteriol*. **188,** 5240–5248.

Platzer, J., Sterr, W., Hausmann, M., and Schmitt, R. (1997). Three genes of a motility operon and their role in flagellar rotary speed variation in *Rhizobium meliloti*. *J. Bacteriol*. **179,** 6391–6399.

Pruss, B. M., and Matsumura, P. (1996). A regulator of the flagellar regulon of *Escherichia coli*, *flhD*, also affects cell division. *J. Bacteriol*. **178,** 668–674.

Pruss, B. M., and Matsumura, P. (1997). Cell cycle regulation of flagellar genes. *J. Bacteriol*. **179,** 5602–5604.

Reid, S. W., Leake, M. C., Chandler, J. H., Lo, C. J., Armitage, J. P., and Berry, R. M. (2006). The maximum number of torque-generating units in the flagellar motor of *Escherichia coli* is at least 11. *Proc. Natl. Acad. Sci. USA* **103,** 8066–8071.

Ryu, W. S., Berry, R. M., and Berg, H. C. (2000). Torque-generating units of the flagellar motor of *Escherichia coli* have a high duty ratio. *Nature* **403,** 444–447.

Sagi, Y., Khan, S., and Eisenbach, M. (2003). Binding of the chemotaxis response regulator CheY to the isolated, intact switch complex of the bacterial flagellar motor: Lack of cooperativity. *J. Biol. Chem*. **278,** 25867–25871.

Samatey, F. A., Imada, K., Nagashima, S., Vonderviszt, F., Kumasaka, T., Yamamoto, M., and Namba, K. (2001). Structure of the bacterial flagellar protofilament and implications for a switch for supercoiling. *Nature* **410,** 331–337.

Samatey, F. A., Matsunami, H., Imada, K., Nagashima, S., Shaikh, T. R., Thomas, D. R., Chen, J. Z., Derosier, D. J., Kitao, A., and Namba, K. (2004). Structure of the bacterial flagellar hook and implication for the molecular universal joint mechanism. *Nature* **431,** 1062–1068.

Samuel, A. D., and Berg, H. C. (1995). Fluctuation analysis of rotational speeds of the bacterial flagellar motor. *Proc. Natl. Acad. Sci. USA* **92,** 3502–3506.

Samuel, A. D., and Berg, H. C. (1996). Torque-generating units of the bacterial flagellar motor step independently. *Biophys. J*. **71,** 918–923.

Sato, K., and Homma, M. (2000a). Functional reconstitution of the Na^+-driven polar flagellar motor component of *Vibrio alginolyticus*. *J. Biol. Chem*. **275,** 5718–5722.

Sato, K., and Homma, M. (2000b). Multimeric structure of PomA, a component of the Na^+-driven polar flagellar motor of *Vibrio alginolyticus*. *J. Biol. Chem*. **275,** 20223–20228.

Schmitt, R. (2002). *Sinorhizobial* chemotaxis: A departure from the enterobacterial paradigm. *Microbiology* **148,** 627–631.

Schmitt, R. (2003). Helix rotation model of the flagellar rotary motor. *Biophys. J.* **85,** 843–852.

Schnitzer, M. J., and Block, S. M. (1997). Kinesin hydrolyses one ATP per 8-nm step. *Nature* **388,** 386–390.

Schoenhals, G. J., and Macnab, R. M. (1996). Physiological and biochemical analyses of FlgH, a lipoprotein forming the outer membrane L ring of the flagellar basal body of *Salmonella typhimurium*. *J. Bacteriol.* **178,** 4200–4207.

Shah, D. S., and Sockett, R. E. (1995). Analysis of the *motA* flagellar motor gene from *Rhodobacter sphaeroides*, a bacterium with a unidirectional, stop-start flagellum. *Mol. Microbiol.* **17,** 961–969.

Shapiro, L., McAdams, H. H., and Losick, R. (2002). Generating and exploiting polarity in bacteria. *Science* **298,** 1942–1946.

Shibata, S., Takahashi, N., Chevance, F. F., Karlinsey, J. E., Hughes, K. T., and Aizawa, S. (2007). FliK regulates flagellar hook length as an internal ruler. *Mol. Microbiol.* **64,** 1404–1415.

Silverman, M., and Simon, M. I. (1974). Flagellar rotation and the mechanism of bacterial motility. *Nature* **249,** 73–74.

Sockett, H., Yamaguchi, S., Kihara, M., Irikura, V., and Macnab, R. M. (1992). Molecular analysis of the flagellar switch protein FliM of *Salmonella typhimurium*. *J. Bacteriol.* **174,** 793–806.

Sourjik, V., and Berg, H. C. (2002). Binding of the *Escherichia coli* response regulator CheY to its target measured *in vivo* by fluorescence resonance energy transfer. *Proc. Natl. Acad. Sci. USA* **99,** 12669–12674.

Sowa, Y., Hotta, H., Homma, M., and Ishijima, A. (2003). Torque-speed relationship of the Na^+-driven flagellar motor of *Vibrio alginolyticus*. *J. Mol. Biol.* **327,** 1043–1051.

Sowa, Y., Rowe, A. D., Leake, M. C., Yakushi, T., Homma, M., Ishijima, A., and Berry, R. M. (2005). Direct observation of steps in rotation of the bacterial flagellar motor. *Nature* **437,** 916–919.

Stader, J., Matsumura, P., Vacante, D., Dean, G. E., and Macnab, R. M. (1986). Nucleotide sequence of the *Escherichia coli* MotB gene and site-limited incorporation of its product into the cytoplasmic membrane. *J. Bacteriol.* **166,** 244–252.

Stallmeyer, B. M. J., Aizawa, S., Macnab, R. M., and DeRosier, D. J. (1989). Image reconstruction of the flagellar basal body of *Salmonella typhimurium*. *J. Mol. Biol.* **205,** 519–528.

Stewart, B. J., and McCarter, L. L. (2003). Lateral flagellar gene system of *Vibrio parahaemolyticus*. *J. Bacteriol.* **185,** 4508–4518.

Stolz, B., and Berg, H. C. (1991). Evidence for interactions between MotA and MotB, torque-generating elements of the flagellar motor of *Escherichia coli*. *J. Bacteriol.* **173,** 7033–7037.

Suzuki, H., Yonekura, K., and Namba, K. (2004). Structure of the rotor of the bacterial flagellar motor revealed by electron cryomicroscopy and single-particle image analysis. *J. Mol. Biol.* **337,** 105–113.

Suzuki, T., and Komeda, Y. (1981). Incomplete flagellar structures in *Escherichia coli* mutants. *J. Bacteriol.* **145,** 1036–1041.

Suzuki, T., Iino, T., Horiguchi, T., and Yamaguchi, S. (1978). Incomplete flagellar structures in nonflagellate mutants of *Salmonella typhimurium*. *J. Bacteriol.* **133,** 904–915.

Tang, H., Billings, S., Wang, X., Sharp, L., and Blair, D. F. (1995). Regulated under-expression and overexpression of the FliN protein of *Escherichia coli* and evidence for an interaction between FliN and FliM in the flagellar motor. *J. Bacteriol.* **177,** 3496–3503.

Tang, H., Braun, T. F., and Blair, D. F. (1996). Motility protein complexes in the bacterial flagellar motor. *J. Mol. Biol.* **261,** 209–221.

Terashima, H., Fukuoka, H., Yakushi, T., Kojima, S., and Homma, M. (2006). The *Vibrio* motor proteins, MotX and MotY, are associated with the basal body of Na^+-driven flagella and required for stator formation. *Mol. Microbiol.* **62,** 1170–1180.

Thomas, D. R., Morgan, D. G., and DeRosier, D. J. (1999). Rotational symmetry of the C ring and a mechanism for the flagellar rotary motor. *Proc. Natl. Acad. Sci. USA* **96,** 10134–10139.

Thomas, D. R., Morgan, D. G., and DeRosier, D. J. (2001). Structures of bacterial flagellar motors from two FliF–FliG gene fusion mutants. *J. Bacteriol.* **183,** 6404–6412.

Thomas, D. R., Francis, N. R., Xu, C., and DeRosier, D. J. (2006). The three-dimensional structure of the flagellar rotor from a clockwise-locked mutant of *Salmonella enterica* serovar *Typhimurium. J. Bacteriol.* **188,** 7039–7048.

Toker, A. S., and Macnab, R. M. (1997). Distinct regions of bacterial flagellar switch protein FliM interact with FliG, FliN and CheY. *J. Mol. Biol.* **273,** 623–634.

Toutain, C. M., Zegans, M. E., and O'Toole, G. A. (2005). Evidence for two flagellar stators and their role in the motility of *Pseudomonas aeruginosa. J. Bacteriol.* **187,** 771–777.

Ueno, T., Oosawa, K., and Aizawa, S. (1992). M ring, S ring and proximal rod of the flagellar basal body of *Salmonella typhimurium* are composed of subunits of a single protein, FliF. *J. Mol. Biol.* **227,** 672–677.

Vogler, A. P., Homma, M., Irikura, V. M., and Macnab, R. M. (1991). *Salmonella typhimurium* mutants defective in flagellar filament regrowth and sequence similarity of FliI to F_OF_1, vacuolar, and archaebacterial ATPase subunits. *J. Bacteriol.* **173,** 3564–3572.

Waters, R. C., O'Toole, P. W., and Ryan, K. A. (2007). The FliK protein and flagellar hook-length control. *Protein Sci.* **16,** 769–780.

Welch, M., Oosawa, K., Aizawa, S. I., and Eisenbach, M. (1993). Phosphorylation-dependent binding of a signal molecule to the flagellar switch of bacteria. *Proc. Natl. Acad. Sci. USA* **90,** 8787–8791.

Wilson, M. L., and Macnab, R. M. (1988). Overproduction of the MotA protein of *Escherichia coli* and estimation of its wild-type level. *J. Bacteriol.* **170,** 588–597.

Wilson, M. L., and Macnab, R. M. (1990). Co-overproduction and localization of the *Escherichia coli* motility proteins MotA and MotB. *J. Bacteriol.* **172,** 3932–3939.

Wolfe, A. J., and Visick, K. L. (2008). Get the message out: Cyclic-di-GMP regulates multiple levels of flagellar-based motility. *J. Bacteriol.* **190,** 463–475.

Wu, J., and Newton, A. (1997). Regulation of the *Caulobacter* flagellar gene hierarchy; not just for motility. *Mol. Microbiol.* **24,** 233–239.

Xing, J., Bai, F., Berry, R., and Oster, G. (2006). Torque-speed relationship of the bacterial flagellar motor. *Proc. Natl. Acad. Sci. USA* **103,** 1260–1265.

Yakushi, T., Maki, S., and Homma, M. (2004). Interaction of PomB with the third transmembrane segment of PomA in the Na^+-driven polar flagellum of *Vibrio alginolyticus. J. Bacteriol.* **186,** 5281–5291.

Yakushi, T., Yang, J., Fukuoka, H., Homma, M., and Blair, D. F. (2006). Roles of charged residues of rotor and stator in flagellar rotation: Comparative study using H^+-driven and Na^+-driven motors in *Escherichia coli. J. Bacteriol.* **188,** 1466–1472.

Yamaguchi, S., Aizawa, S., Kihara, M., Isomura, M., Jones, C. J., and Macnab, R. M. (1986a). Genetic evidence for a switching and energy-transducing complex in the flagellar motor of *Salmonella typhimurium. J. Bacteriol.* **168,** 1172–1179.

Yamaguchi, S., Fujita, H., Ishihara, H., Aizawa, S., and Macnab, R. M. (1986b). Subdivision of flagellar genes of *Salmonella typhimurium* into regions responsible for assembly, rotation, and switching. *J. Bacteriol.* **166,** 187–193.

Yamashita, A., Singh, S. K., Kawate, T., Jin, Y., and Gouaux, E. (2005). Crystal structure of a bacterial homologue of Na^+/Cl^--dependent neurotransmitter transporters. *Nature* **437,** 215–223.

Yamashita, I., Hasegawa, K., Suzuki, H., Vonderviszt, F., Mimori-Kiyosue, Y., and Namba, K. (1998). Structure and switching of bacterial flagellar filaments studied by X-ray fiber diffraction. *Nat. Struct. Biol.* **5,** 125–132.

Yasuda, R., Noji, H., Kinosita, K., Jr., and Yoshida, M. (1998). F$_1$-ATPase is a highly efficient molecular motor that rotates with discrete 120 degree steps. *Cell* **93,** 1117–1124.

Yonekura, K., Maki, S., Morgan, D. G., DeRosier, D. J., Vonderviszt, F., Imada, K., and Namba, K. (2000). The bacterial flagellar cap as the rotary promoter of flagellin self-assembly. *Science* **290,** 2148–2152.

Yonekura, K., Maki-Yonekura, S., and Namba, K. (2003). Complete atomic model of the bacterial flagellar filament by electron cryomicroscopy. *Nature* **424,** 643–650.

Yonekura, K., Yakushi, T., Atsumi, T., Maki-Yonekura, S., Homma, M., and Namba, K. (2006). Electron cryomicroscopic visualization of PomA/B stator units of the sodium-driven flagellar motor in liposomes. *J. Mol. Biol.* **357,** 73–81.

Yorimitsu, T., and Homma, M. (2001). Na$^+$-driven flagellar motor of *Vibrio. Biochim. Biophys. Acta* **1505,** 82–93.

Yorimitsu, T., Asai, Y., Sato, K., and Homma, M. (2000). Intermolecular cross-linking between the periplasmic Loop3–4 regions of PomA, a component of the Na$^+$-driven flagellar motor of *Vibrio alginolyticus. J. Biol. Chem.* **275,** 31387–31391.

Yorimitsu, T., Sowa, Y., Ishijima, A., Yakushi, T., and Homma, M. (2002). The systematic substitutions around the conserved charged residues of the cytoplasmic loop of Na$^+$-driven flagellar motor component PomA. *J. Mol. Biol.* **320,** 403–413.

Yorimitsu, T., Mimaki, A., Yakushi, T., and Homma, M. (2003). The conserved charged residues of the C-terminal region of FliG, a rotor component of the Na$^+$-driven flagellar motor. *J. Mol. Biol.* **334,** 567–583.

Yorimitsu, T., Kojima, M., Yakushi, T., and Homma, M. (2004). Multimeric structure of the PomA/PomB channel complex in the Na$^+$-driven flagellar motor of *Vibrio alginolyticus. J. Biochem. (Tokyo)* **135,** 43–51.

Zhao, R., Amsler, C. D., Matsumura, P., and Khan, S. (1996a). FliG and FliM distribution in the *Salmonella typhimurium* cell and flagellar basal bodies. *J. Bacteriol.* **178,** 258–265.

Zhao, R., Pathak, N., Jaffe, H., Reese, T. S., and Khan, S. (1996b). FliN is a major structural protein of the C-ring in the *Salmonella typhimurium* flagellar basal body. *J. Mol. Biol.* **261,** 195–208.

Zhou, J., and Blair, D. F. (1997). Residues of the cytoplasmic domain of MotA essential for torque generation in the bacterial flagellar motor. *J. Mol. Biol.* **273,** 428–439.

Zhou, J., Fazzio, R. T., and Blair, D. F. (1995). Membrane topology of the MotA protein of *Escherichia coli. J. Mol. Biol.* **251,** 237–242.

Zhou, J., Lloyd, S. A., and Blair, D. F. (1998a). Electrostatic interactions between rotor and stator in the bacterial flagellar motor. *Proc. Natl. Acad. Sci. USA* **95,** 6436–6441.

Zhou, J., Sharp, L. L., Tang, H. L., Lloyd, S. A., Billings, S., Braun, T. F., and Blair, D. F. (1998b). Function of protonatable residues in the flagellar motor of *Escherichia coli*: A critical role for Asp 32 of MotB. *J. Bacteriol.* **180,** 2729–2735.